LITHIUM LENS (II)
LITHIUM FLOW MAGNETO-HYDRODYNAMICS

A.Mikhailichenko, Cornell University, LEPP, Ithaca, NY 14853

Abstract

We continue our investigation of Lithium Lens (LL) for usage in ILC positron conversion system. Magneto-Hydrodynamic and Thermo-dynamic problems discussed in association with ~100 kA feeding pulsed current. Set of Partial Differential Equations used for description of magneto-hydrodynamics phenomena in liquid Lithium flow. Calculations confirm feasibility of liquid Lithium system. Some interesting phenomena (such as circulation in central region and some others) discovered in Lithium flow.

OVERVIEW

In our previous publication [1] we introduced LL design, including the engineering aspects such as overall configuration, windows attachment and alignment concept.

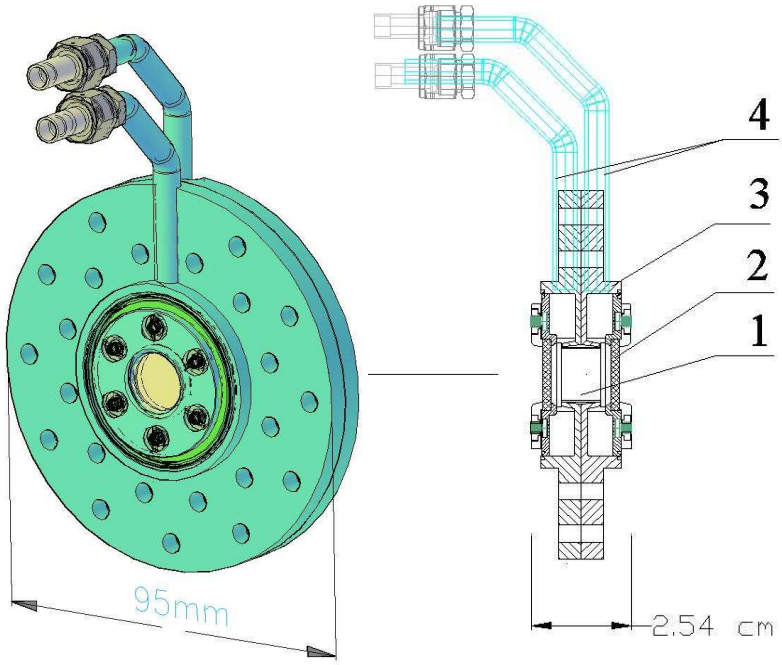

Figure 1: Lithium Lens for ILC positron source; extended flanges serve for electrical contact. 1–volume with Lithium, 2–window (Be/BC/BN), 3–electrical contacts with caverns for Li, 4–tubing for Lithium in/out [2].

One characteristic peculiarity of this design (besides usage of liquid Lithium) is the extended buffer toroid-like volume which serves for redistribution of flow in the central region evenly. Thickness of windows was chosen to be big enough to withstand pressure of ~20 atm. BN, BC and Beryllium-are candidates for material of this window [1].

PRELIMINARY REMARKS

Set of equations used for modeling could be grouped into three categories: *Electromagnetic*, *Hydrodynamic* and *Thermodynamic*. All three have cross terms linking electric current, fluid flow and temperature relaxation due to thermo-conductivity, Ohmic heating, fluid motion and frictional heat generation due to viscose phenomena. When compessivity is included in the set of equations, the equation of state is required for balancing the self consistency.

Electromagnetic:

As we are planning to have *voltage* applied to the lens as a given parameter, we have chosen solution through vector-scalar potentials:

$$\vec{E} = -\frac{\partial \vec{A}}{\partial t} - grad(U); \quad \vec{B} = rot(\vec{A}); \quad \vec{j} = \sigma \cdot (\vec{E} + \vec{v} \times \vec{B}); \quad \vec{B} = \mu \cdot \vec{H} \tag{1}$$

$$div(\vec{j}) = 0 \tag{2}$$

$$div(grad(A_x)) + \mu \cdot j_x = 0 \qquad div(grad(A_y)) + \mu \cdot j_y = 0 \qquad div(grad(A_z)) + \mu \cdot j_z = 0, \tag{3}$$

where $\mu = \mu_0 \mu_r$, $\mu_0 \cong 4\pi \cdot 10^{-7} H/m$; μ_r is relative permeability (μ_r =1 in our model), $\vec{v}$ stands for the local velocity, σ is electric conductivity. The last set of equations (3) means that we are using Coulomb calibration.

Total energy deposition into the lens by feeding current during time ΔT can be calculated as

$$\Delta Q_{tot} = \int_0^{\Delta T} dt \int_V (\vec{j} \cdot \vec{E}) dV = \int_0^{\Delta T} dt \int_V \frac{j^2}{\sigma} dV .$$

We will represent this number for single pulse which corresponds to the integration time > 2.3msec. Total losses associated with the single pulse are ~682 *Joules* arriving to 3.4 *kW* for 5 *Hz* operation rate for ~70 kA feeding current.

Hydrodynamic :

General equations describing the transport of momentum can be written as the following [3]-[5][1]

$$\frac{\partial}{\partial t} \rho v_i = -\frac{\partial \Pi_{ik}}{\partial x_k}, \tag{4}$$

where momentum flux density tensor can be represented as [4]

$$\Pi_{ik} = P \cdot \delta_{ik} + \rho \cdot v_i v_j - \sigma'_{ik} - \mu_0 (H_i H_k - \tfrac{1}{2} H^2 \delta_{ik}), \tag{5}$$

First term is associated with volume distribution of pressure. Second term s associated with fluid motion and could be treated as dynamic pressure. Deviatoric stress tensor $\sigma'_{ij}(\vec{r},t)$ is a part of tensor of momentum flux density responsible for transferring of momentum by viscose forces [3]. This tensor can be expressed as the following

[1] Einstein's summation rule is in action.

$$\sigma'_{ij} = \eta\left(\frac{\partial v_i}{\partial x_j} + \frac{\partial v_j}{\partial x_i} - \tfrac{2}{3}\delta_{ij}\frac{\partial v_k}{\partial x_k}\right) + \zeta \cdot \delta_{ij}\frac{\partial v_k}{\partial x_k} \tag{6}$$

reduced in uncompressible flow to

$$\sigma'_{ij} = \eta\left(\frac{\partial v_i}{\partial x_j} + \frac{\partial v_j}{\partial x_i}\right) \tag{7}$$

Components of this tensor define stress in liquid generated by viscose flow, i.e. it is responsible for transferring momenta in fixed direction at some depth, when the slice of fluid above this slice is in motion. Losses in liquid per second by viscosity defined by this term as $\sigma'_{ij} \cdot \frac{\partial v_i}{\partial x_j}$. Energy dissipation rate in *whole* lens on can obtain by integration of this term over whole volume occupied by Lithium

$$\frac{d\varepsilon}{dt} = -\oint_V \sigma'_{ij} \cdot \frac{\partial v_i}{\partial x_j} dV = -\frac{1}{2}\oint_V \sigma'_{ij} \cdot \left(\frac{\partial v_i}{\partial x_j} + \frac{\partial v_j}{\partial x_i}\right) dV \tag{8}$$

For uncompressible flow one can use (7) and substitute it in (8) arriving to

$$\frac{d\varepsilon}{dt} = -\oint_V \sigma'_{ij} \cdot \frac{\partial v_i}{\partial x_j} dV = -\frac{\eta}{2}\oint_V \left(\frac{\partial v_i}{\partial x_j} + \frac{\partial v_j}{\partial x_i}\right)^2 dV \tag{9}$$

Motion of liquid defined by (4) after substitution there (5)

$$\rho \cdot \left(\frac{\partial v_i}{\partial t} + v_j \frac{\partial v_i}{\partial x_j}\right) + \frac{\partial P}{\partial x_i} = (\vec{j} \times \vec{B})_i + \frac{\partial}{\partial x_j}\left[\eta\left(\frac{\partial v_i}{\partial x_j} + \frac{\partial v_j}{\partial x_i} - \tfrac{2}{3}\delta_{ij}\frac{\partial v_k}{\partial x_k}\right)\right] + \frac{\partial}{\partial x_i}\left(\zeta \cdot div(\vec{v})\right), \tag{10}$$

where δ_{ij} is Kronecker delta, η stands for viscosity, $\zeta = \lambda + \frac{2}{3}\eta$, λ is a second coefficient of viscosity (we are not using this coefficient in our calculations).

For uncompressible flow $div(\vec{v}) \equiv \partial v_k / \partial v_k = 0$ and equations of liquid motion reduced to the

$$\begin{aligned}
&\rho \cdot \left(\frac{\partial v_x}{\partial t} + v_x\frac{\partial v_x}{\partial x} + v_y\frac{\partial v_x}{\partial y} + v_z\frac{\partial v_x}{\partial z}\right) + \frac{\partial P}{\partial x} - \eta \cdot div(grad(v_x)) = (\vec{j} \times \vec{B})_x \\
&\rho \cdot \left(\frac{\partial v_y}{\partial t} + v_x\frac{\partial v_y}{\partial x} + v_y\frac{\partial v_y}{\partial y} + v_z\frac{\partial v_y}{\partial z}\right) + \frac{\partial P}{\partial y} - \eta \cdot div(grad(v_y)) = (\vec{j} \times \vec{B})_y \\
&\rho \cdot \left(\frac{\partial v_z}{\partial t} + v_x\frac{\partial v_z}{\partial x} + v_y\frac{\partial v_z}{\partial y} + v_z\frac{\partial v_z}{\partial z}\right) + \frac{\partial P}{\partial z} - \eta \cdot div(grad(v_z)) = (\vec{j} \times \vec{B})_z
\end{aligned} \tag{11}$$

In vector form these can be rewritten as

$$\rho \cdot \left(\frac{\partial \vec{v}}{\partial t} + (\vec{v} \cdot \vec{\nabla})\vec{v}\right) + grad(P) - \eta \cdot \nabla^2 \vec{v} = (\vec{j} \times \vec{B}). \tag{12}$$

If compression is not neglected but variation of viscosity along the flow is small, then equations (4) can be reduced to

$$\rho\cdot(\frac{\partial\vec{v}}{\partial t}+(\vec{v}\cdot\vec{\nabla})\vec{v}+grad(P)-\eta\cdot\nabla^2\vec{v}-\left(\zeta+\tfrac{1}{3}\eta\right)grad(div(\vec{v}))=(\vec{j}\times\vec{B}). \qquad (13)$$

Without term at the right side, $(\vec{j}\times\vec{B})=0$, expression (13) in known as Navier-Stokes equation. For pressure we used an equation obtained from (13) while applied operand divergence to it

$$div(grad(P))\left\{-\frac{1}{c_B^2}\frac{\partial^2 P}{\partial t^2}\right\}=div(\vec{j}\times\vec{B})-\rho\cdot div\left(\frac{\partial\vec{v}}{\partial t}+(\vec{v}\cdot\vec{\nabla})\vec{v}\right)+C\eta\cdot div(\vec{v})\left\{-\Gamma\cdot\ddot{Q}(\vec{r},t)\right\}, \qquad (14)$$

where $\boldsymbol{\Gamma}$ is Grüneisen coefficient, C is arbitrary constant. By brackets { } marked terms not involved in calculation is this current investigation, but will be used when beam –lens interaction will be under consideration. Term $Q(\vec{r},t)$ defines profile of energy density deposition by the beam. Term with second derivative becomes important at times $t<L/c_B\cong 10\mu s$, i.e. for excitation by single bunch in train.

Let us estimate action of magnetic field to the pressure using equation (12). For steady conditions in non-viscous flow at the top of feeding current equation (12) reduced to

$$\vec{\nabla}(P)=(\vec{j}\times\vec{B}) \qquad (15)$$

One can expand these equations in cylindrical coordinates as

$$\vec{\nabla}P\cong\frac{dP}{dr}=j_z B_\vartheta(r)=\frac{\mu_0 j_z^2}{2}r, \qquad (16)$$

where it was substituted $B_\vartheta(r)=\mu_0 H_\vartheta(r)\cong\mu_0 Ir/(2\pi a^2)$, where a stands for the radius of Lithium flow at central part. Maximal field value reached at the surface goes to be

$$B_{\max}(r=a)\cong\frac{\mu_0 I}{2\pi a}\cong\frac{\mu_0 a\cdot j_z}{2} \qquad (17)$$

We can set the pressure at the surface equal to zero (free surface) which is valid for solid Lithium rod, so

$$P(r)=\frac{\mu_0 j_s^2}{4}(a^2-r^2)=\frac{1}{\mu_0}\frac{\mu_0^2 j_s^2 a^2}{4}(1-\frac{r^2}{a^2})=\frac{B_{\max}^2}{\mu_0}(1-\frac{r^2}{a^2})=P_0\cdot(1-\frac{r^2}{a^2}). \qquad (18)$$

Substitute for estimations $I=\oiint j_z dS\cong j_z\pi\cdot a^2\cong 70kA$, a=0.5cm, one can evaluate

$$B_{\max}\cong\frac{\mu_0 I}{2\pi a}\cong\frac{4\pi\cdot 10^{-7}\cdot 7\cdot 10^4}{2\pi\cdot 0.5\cdot 10^{-2}}\cong 2.8\ T.$$

As $1T\leftrightarrow\cong 4atm$, the pressure at the center part of lens comes to be $P_0\cong 31atm\cong 3\cdot 10^6 Pa$. This is a pressure prop between periphery and central region. In our model the pressure drop between inlet/outlet tube fringe was varied up to **p_in=2E6** Pa (i.e. ~20atm), while at the middle of lens it comes to ~half of this value i.e. to $1\cdot 10^6 Pa$, so the magneto-pressure influences substantially to the flow as it will be confirmed by numerical calculations.

Situation when liquid Lithium is in use is quite different compared with solid Lithium usage. Namely when magnetic pressure applied to the solid Lithium there is a possibility for development a gap between Lithium surface and the inner surface of container. Indeed, in case of liquid the liquid has a tendency to fill this gap by supplied portions from inlet hose. In modeling we set the boundary conditions as **natural(p)=0** which means absence of flux through boundary (see below).

Thermodynamic:

Temperature dynamics defined by balance of energy in moving media. From thermodynamic identity $d\varepsilon = TdS - PdV = TdS + \frac{P}{\rho^2} d\rho$ could be derived the balance entropy *S*. Using identities $T\frac{\partial S}{\partial t} = C_p \frac{\partial T}{\partial t}$ and $T \cdot div(s) = C_p grad(T)$ [5] one can obtain equation for temperature as the following

$$\rho \cdot C_p \left(\frac{\partial T}{\partial t} + \vec{v} \cdot grad(T) \right) - div(k \cdot grad(T)) + P \cdot div(\vec{v}) = (\vec{j} \cdot \vec{E}) + \sigma'_{ik} \frac{\partial v_i}{\partial x_k} + \dot{Q}(\vec{r}, t), \qquad (19)$$

k is thermal conductivity, C_p is heat capacity, ρ is volume density of Lithium.

Let us make preliminary evaluation of terms $\sigma'_{ij} \cdot \frac{\partial v_i}{\partial x_j}$ and $(\vec{j} \cdot \vec{E})$ at maximum current.

$$\left.\frac{d\varepsilon}{dt}\right|_{vis} \cong -\eta \oint_V \left(\frac{\partial v_i}{\partial x_j} \right)^2 dV \cong -\eta \left(\frac{\partial v_i}{\partial x_j} \right)^2 L \cdot S \approx -\frac{\eta v^2 \cdot S}{L} \approx -\pi \eta v^2 \cdot L \qquad (20)$$

where $S \cong \pi L^2$ stands for cross section of flow. Velocity of flow in central part of lens could be found as big as *v*~100 m/sec (at max, when term $(\vec{j} \times \vec{B})$ is acting) viscosity of Lithium at 573K is η~5.2E-4 Pa-s [6] , so the term associated with viscosity comes to be for characteristic dimension *L*~1*cm*

$$\left.\frac{d\varepsilon}{dt}\right|_{vis} \cong -3.14 \cdot 5.2 \cdot 10^{-4} \cdot 10^4 \cdot 10^{-2} \approx -1.6 \cdot 10^{-2} [W/m^3].$$

Meanwhile the Ohmic losses could be expressed as

$$\left.\frac{d\varepsilon}{dt}\right|_{Ohmic} \cong -\frac{1}{\sigma} \oint_V j^2 dV \cong -\frac{1}{\sigma} I^2 \frac{LS}{S^2} \approx \frac{I^2}{\pi \sigma L} \ . \qquad (21)$$

Substitute in last formula numerical values for current *I*=100*kA*, $\sigma = 3 \cdot 10^6 [Ohm^{-1} \cdot m^{-1}]$ one can obtain

$$\left.\frac{d\varepsilon}{dt}\right|_{Ohmic} \approx -\frac{100^2 10^6}{3.14 \cdot 3 \cdot 10^6 0.01} \cong -10^5 [W/m^3].$$

So the Ohmic losses (and heating) one could expect to be much more severe, than the ones arising from viscosity. So although the terms with viscosity dissipation included in general model, we sometimes turned off these ones to speed up the calculations.

Expression for viscosity loss term used in model (named as **pfi** in equation on page 9) is

$$phi = \sigma'_{ij}\frac{\partial v_i}{\partial x_j} = \eta\frac{\partial v_i}{\partial x_j}\left[\left(\frac{\partial v_i}{\partial x_j}+\frac{\partial v_j}{\partial x_i}-\tfrac{2}{3}\delta_{ij}\frac{\partial v_k}{\partial x_k}\right)+\zeta\cdot\delta_{ij}\frac{\partial v_k}{\partial x_k}\right]=$$

$$2\eta\left[\left(\frac{\partial v_x}{\partial x}\right)^2+\left(\frac{\partial v_y}{\partial y}\right)^2+\left(\frac{\partial v_z}{\partial z}\right)^2+\frac{1}{2}\left(\frac{\partial v_x}{\partial y}+\frac{\partial v_y}{\partial x}\right)^2+\frac{1}{2}\left(\frac{\partial v_y}{\partial z}+\frac{\partial v_z}{\partial y}\right)^2+\frac{1}{2}\left(\frac{\partial v_z}{\partial x}+\frac{\partial v_x}{\partial z}\right)^2+\zeta\cdot(div(\vec{v}))^2\right] \quad (22)$$

Distribution of losses calculated with this formula represented in Fig. 43, see below. Physical meaning of this heat generation lies in fact that for liquid, viscosity phenomena equivalent motion with friction as the layers of liquid interacts through normal to direction of motion surface. So the friction forces responsible for heat deposited described by this term (22).

One can see from equation (12) that for influence viscose term relatively to kinematics of liquid one should compare terms

$$\rho\cdot\frac{\partial\vec{v}}{\partial t}\cong\frac{\rho v}{\tau}\quad\text{and}\quad\eta\cdot\nabla^2\vec{v}\cong\frac{\eta v}{r^2}. \quad (23)$$

Ratio of these terms is ***Reynolds number***

$$\mathrm{Re}=\frac{\rho v/\tau}{\eta v/r^2}=\frac{\rho\cdot r^2}{\tau\eta}\cong\frac{\rho\cdot v\cdot r}{\eta}, \quad (24)$$

where was substituted $r\cong v\tau$, r stands for characteristic distance and τ stands for characteristic time scale of process. For our parameters r~1cm, v~1m/s viscosity $\eta\cong 5\cdot10^{-4}\,Pa\cdot s$, $\rho\cong 0.5\cdot10^3 kg/m^3$, $\mathrm{Re}\cong\frac{0.5\cdot10^3[kg/m^3]\cdot0.1[m/\sec]\cdot10^{-2}[m]}{5\cdot10^{-4}[N/m^2\cdot\sec]}\cong10^3$. This means that Lithium motion is turbulent brining problems with modeling, as there is no steady solution for the flow.

Magnetic Reynolds parameter defined in magneto-hydrodynamics as a ratio of characteristic dimension to the depth of skin layer [4] (see equations (1)-(3) and (29) below)

$$\mathrm{Re}_m=\frac{r}{\delta_e}=\frac{r\sqrt{\mu\sigma}}{\sqrt{\tau}} \quad (25)$$

in our case Re_m~1. In the same manner one can introduce ***Thermo Reynolds*** number as a ratio of characteristic dimension to the thermal skin layer thickness (see (19));

$$\mathrm{Re}_T=\frac{r}{\delta_T}=\frac{v\tau}{\left(\frac{\sqrt{k\tau}}{\sqrt{\rho C_p}}\right)}\cong\frac{v\sqrt{\tau\rho C_p}}{\sqrt{k}} \quad (26)$$

First, let us estimate thermal skin layer depth $\delta_T=\sqrt{k\tau}/\sqrt{\rho C_p}$. Substitute here k=43.15 *W/m-K*, C_p=4.38 kJ/kg/^{o}K, one can obtain

$$\delta_T\cong\frac{\sqrt{43\cdot10^{-3}}}{\sqrt{0.5\cdot10^3 4.38\cdot10^3}}=1.4\cdot10^{-4}m,$$

while $v\tau\cong0.1[m/\sec]\cdot10^{-3}[\sec]\cong10^{-4}m$, i.e. Re_T~1. This means that for one millisecond thermal diffusion is of the order of flow distance.

NUMERICAL MODEL

All equations represented in previous section are used for modeling of Liquid Lithium flow. For modeling with these equations, Partial Differential Equation solver FlexPDE [8] is used. As it could be concluded from description of this software, it uses Galerkin method on the basis of trigonometric polynomials. This solver uses then modified Newton Raphson iteration procedure. This code allows easy access to the problem script and it is user friendly. Other possibilities might be associated with the COMSOL and ANSYS; these both have solvers for fluid motion.

3D model was erected, some imperfections (such as ~0.1mm shift of Lithium central part and feeding tubes) was modeled. Although inlet and outlet tubes attached in slightly different style as in our engineering model, this does not influence results and was just made for simplification. What is important here is that viscose phenomena mostly effectively manifested exactly at the inlet and outlet tubes, where reduction of velocity is substantional, despite the input pressure kept at the level of 1-10*atm*.

FlexPDE divides the volume mesh in accordance of accuracy required; the accuracy is merely a matter of time. We did not uses extreme values, as the 10% accuracy is more than enough for most realistic conditions. As velocity is much different in different parts of lens, Reynolds number serves just for general characterization of Lithium flow (for example velocity comes to zero at the inner surface). In our model we used maximal value of velocity over all volume and the size of model as a characteristic dimension: **RE=density*globalmax(vm)*2*L/visc** , where **vm** stands for velocity modulus. So this number is a major one for the problem at any time.

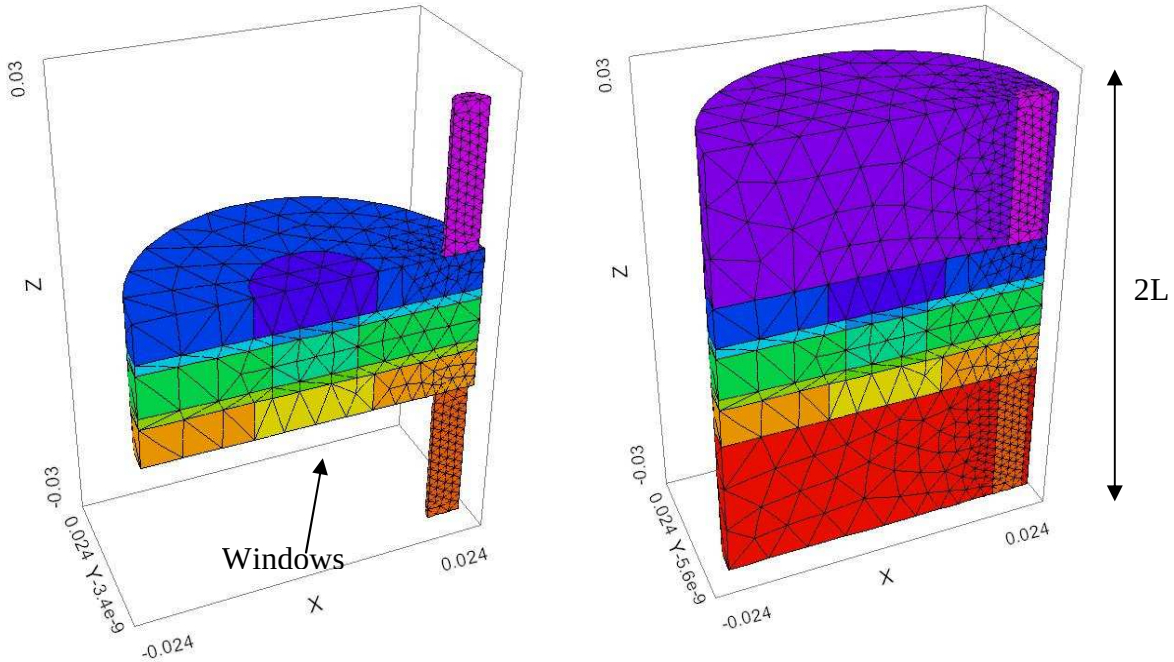

Figure2: Model 1 and Model 2 use the same equations; model 2 has no mesh in upper and lower layers, sometimes we excluded even volume occupied by windows.

As one could see, the full problem is a set of differential equations, in which instant values of variables from one equation used in another as given and vice versa. So this becomes complicated nonlinear problem, sensitive to the sequence of equations to be solved. Time dependence adds to complexity, as the time step of one variable propagates through the model by appropriate algorithm, which is sensitive to the values of others variables, time step itself and spatial division of model (mesh size). For pure hydrodynamic part of equation set the model could be simplified by excluding

the regions where the Lithium is not flowing. For calculation of magnetic field we using vector-scalar potentials which have boundary conditions of rather different nature, so for simplicity we restore the grid in layers having feeding tubes and the ones reserved for windows. So we used two grid systems for our problem depending of problem to be solved.
Volume represented at the right required for easier satisfaction of boundary conditions for vector potential. For heat and liquid transport this volumes at the top and bottom of model could be voided. In full model we set viscosity, heat conductivity electric conductivity in volume where there is no material as

layer 'down' sigma=1e-15 visc=1e10 k=1e-15 density=1e10
layer 'up' sigma=1e-15 visc=1e10 k=1e-15 density=1e10

which stands for $\sigma = 10^{15} Ohm^{-1} m^{-1}$, $\eta = 10^{10}\ Pa \cdot s$, $k = 10^{-15} W/K/m$, $\rho = 10^{10} kg/m^3$

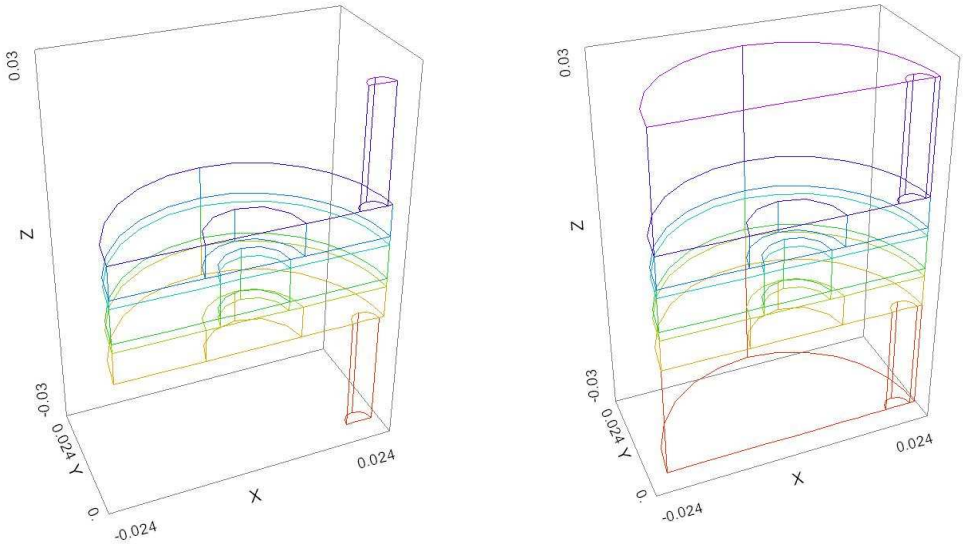

Figure3: 3D sketch of model as it appears in FlexPDE.

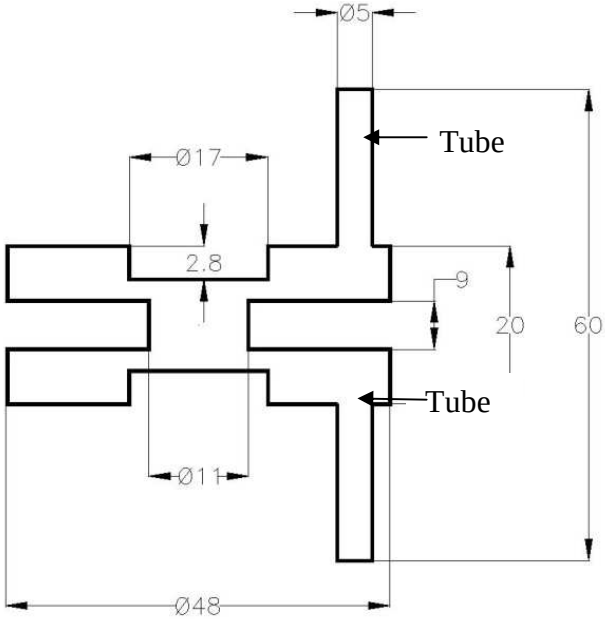

Figure 4: Dimensions of model, *mm*. All dimensions are subject of optimization process.

Accuracy of calculations set within 10^{-3}-10^{-4} for most variables which are velocity, vector-potential, scalar potential, pressure, temperature (plus time derivative of pressure, not used in this series of calculations, but will be used in modeling with beam).
Dimensions for modeling cover $L=\pm 3cm$ in vertical direction; radius of model $Ra=2.4$ *cm*; other dimensions given in Fig.4 above.

Variables and parameters

Variables are: three components of velocity (vector $\vec{v}$), three components of vector-potential (vector $\vec{A}$), temperature T and pressure P.

v(1e-2)=vector(vx,vy,vz) A(1.e-3)=vector(Ax,Ay,Az) U(1e-3) P(1e-2) Temp (1e-3) !dpt(1e-3)

Other numerical parameters used for this modeling are [6] (temperature in Kelvin)

$$\rho = 278.5 - 0.04657 \cdot T + 274.6 \cdot \left(1 - \frac{T}{3500}\right)^{0.467}, \quad kg/m^3$$

$$k = 22.28 + 0.05 \cdot T - 1.243 \cdot 10^{-5} \cdot T^2, \quad W/m/^oK$$

$$\sigma = 10^9 / \left(-64.9 + 1.064 \cdot T - 1.035 \cdot 10^{-3\cdot} \cdot T^2 + 5.33 \cdot 10^{-7} \cdot T^3 - 9.23 \cdot 10^{12} \cdot T^4\right), \ Ohm^{-1}m^{-1}$$

$$C_p = 4754 - 0.925 \cdot T + 2.91 \cdot 10^{-4} \cdot T^2, \ J/kg/^oK$$

$$\eta = \exp\left(-4.164 - 0.6374 \cdot \ln T + 292.1/T\right) Pa \cdot s$$

For temperature 473^{o}K (200^{o}C; melting temperature of Lithium is 454 ^{o}K or ~181^{o}C)), this comes to $\eta = 5.686 \cdot 10^{-4}\ Pa \cdot s$. In [7] represented slightly different approximation of viscosity based on measurements by oscillating-cup vicousemeter in temperature range from 464 to 923 K as

$$\eta = 1.522 \cdot 10^{-4} \cdot \exp(703.66/T)$$

For temperature 473^{o}K this formula gives $\eta \cong 6.74 \cdot 10^{-4}$ *Pa-s*. The difference lies below the accuracy of calculations.

Initial values

vx=0 vy=0 vz=0 P=1e6 Temp=Ta+(Tb-Ta)*(z+L)/2/L or Temp=Ta

so the initial temperature is linearly varying from inlet to outlet from value **Ta** to **Tb.** In latest set of runs, temperature of all walls along the model was chosen to be 480 ^{o}C.

Tuning of model

First, it was necessary to choose initial pressure and pressure drop actoss inlet/outle tube orifices. In time predecessing appearance electric current it is easy to arrange steady flow. Pressure chisen of the order of few atmosperes and pressure drop settled articficially in some margings to obtain a stedy flow (what defined basically just by pressure drop across model).
For exclusion of Gibbs phenomena some artificial diffusion was introduced. It based on including terms with **~div(v)** in equations, for uncompressible flow this term is zero, but gives some decrement. Anouther way to controll calculations in FlexPDE is usage of opernd **THEN .** In sequence of equations it plays role of distributor of sequence within one step of calculations with few equations. Namely, the text in script with operand **THEN** looks like

EQUATIONS
U: div(J)=0.
A: div(grad(A))=0
THEN
v: density*(dt(v)+dot(v,grad(v)))+grad(p)-visc*div(grad(v))=cross(J,B) +visc/3*grad(div(v))
p: div(grad(p))=density*div(dt(v)+dot(v,grad(v)))+div(cross(J,B))+1e5*visc/r^2*div(v)
+visc/3*div(grad(div(v))) !+1/c02*dt(dpt)!-G/c02*Q
Temp: density*cp*(dt(Temp)+dot(v,grad(Temp)))-k*div(grad(Temp))+p*div(v)=dot(J,E) +pfi

pfi stands for set of terms described by (22). Each set of equations solved one by one; while solving the set within **THEN**, the variables in other equations hold constant during one time step. Equations are the same in two models. Except the one with omitted mesh at lower and upper layers and in grooves for windows used for hydrodynamical calculations only.

PRESSURE DYNAMICS

Pressure set at input and output orifices of Lithium duct at the model boundary as **value(p)=p_in**, **value(p)=p_out** respectively. Boundary conditions for pressure in modeling with FlexPDE electric feeding pulse heating defined as $\boldsymbol{natural(P) = \partial P / \partial n}$, where

$$\frac{\partial P}{\partial n} = n_x \cdot \left[(\vec{j} \times \vec{B})_x + \eta \cdot div(grad(v_x) - \rho \cdot (\frac{\partial v_x}{\partial t} + v_x \frac{\partial v_x}{\partial x} + v_y \frac{\partial v_x}{\partial y} + v_z \frac{\partial v_x}{\partial z}) \right] +$$
$$n_y \cdot \left[(\vec{j} \times \vec{B})_y + \eta \cdot div(grad(v_y) - \rho \cdot (\frac{\partial v_y}{\partial t} + v_x \frac{\partial v_y}{\partial x} + v_y \frac{\partial v_y}{\partial y} + v_z \frac{\partial v_y}{\partial z}) \right] + \qquad (27)$$
$$n_z \cdot \left[(\vec{j} \times \vec{B})_z + \eta \cdot div(grad(v_z) - \rho \cdot (\frac{\partial v_z}{\partial t} + v_x \frac{\partial v_z}{\partial x} + v_y \frac{\partial v_z}{\partial y} + v_z \frac{\partial v_z}{\partial z}) \right] +$$

For inlet tube pressure is set to **P_in=1E6** P*a*, for outlet one it is set to zero. Boundary condition for velocity at the inner surface of the lens are set as $\vec{v} = \boldsymbol{vector}(0,0,0)$, so there is no sliding along the surface. This could be easily modified, however, if necessary.

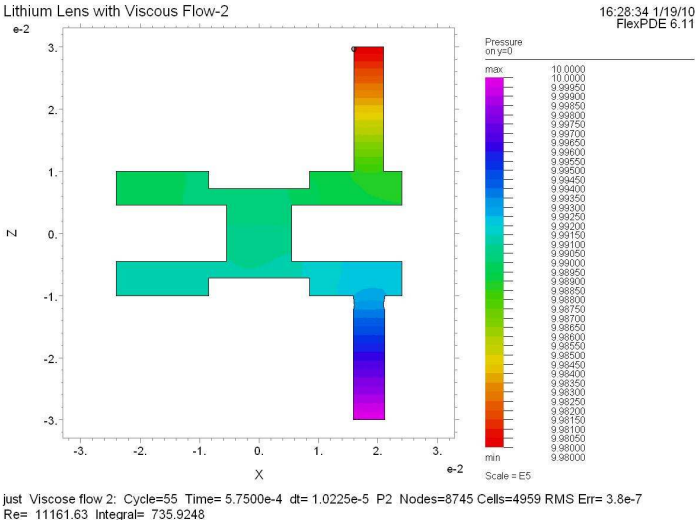

Figure 5: Pressure without electric current.

During modeling relative orientation of inlet and outlet tubes was varied just for understanding the dependence. With skew symmetrical orientation the temperature and pressure variation was minimal, but mirror symmetry induced by design, yield slight bigger asymmetry, which was found acceptable. Each time dependent picture could be represented as a movie. Size of file with results for ~12*msec* calculations occupies ~7.9 GB and takes ~7 hours of calculation on PC with quad processor with multi-thread (4 threads) processing.
While full model is in use the pressure at the boundaries transferred through, so it appears in regions, where materials are absent. This happens as we did not surround Lithium by container which holds the pressure.

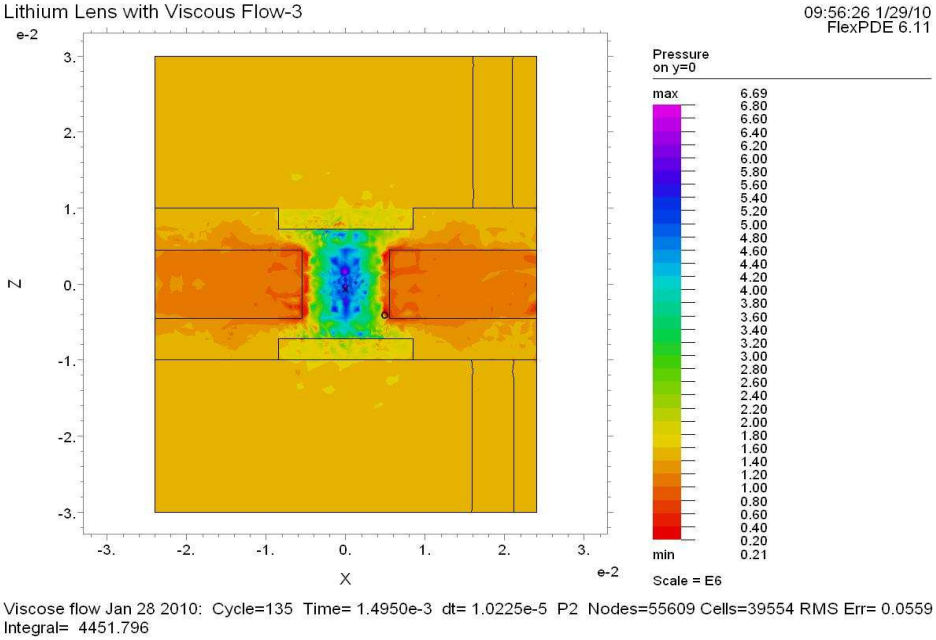

Figure 6: Pressure in volume while current is running.

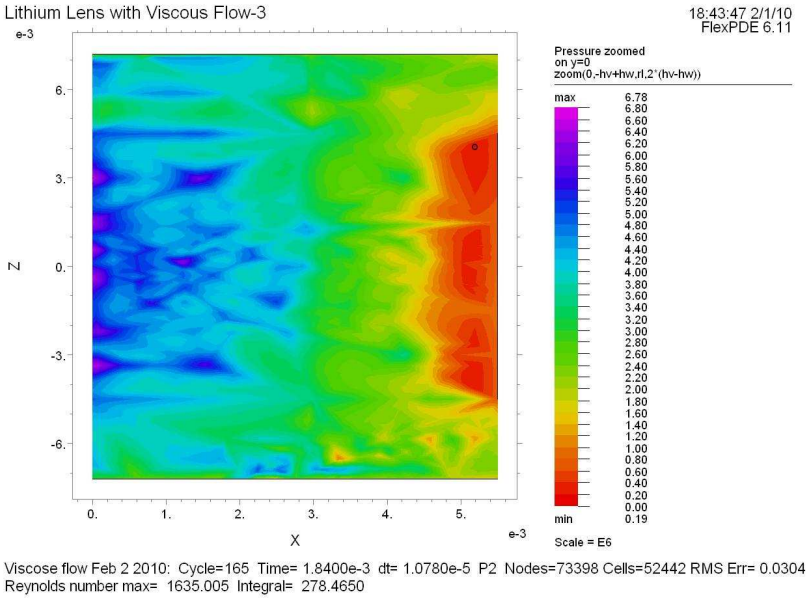

Figure 7: Pressure from previous Figure zoomed at central region, term $\vec{J} \times \vec{B}$ in on. Inlet pressure **p_in=1.5e6** *Pa*, **delp=1.5e4** *Pa*. Left side of this plot considers with axis of flow from window to window. Time ~1.84 *msec* from beginning of process.

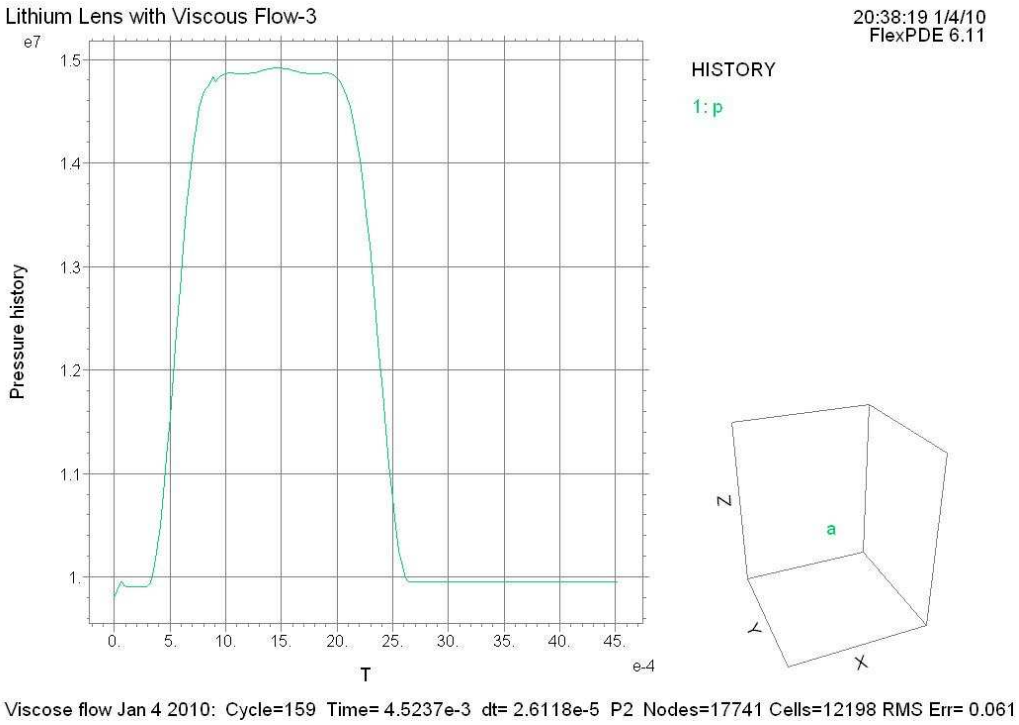

Figure 8: History of pressure at central point. One can see that pressure jumps ~1.5 times in this run.

ELECTRIC CURRENT FLOW

Substitute in equation (2) values of current from (1) one can obtain

$$div(\vec{j}) = -\left(div(\boldsymbol{\sigma} \cdot \frac{\partial \vec{A}}{\partial t}) + div(\boldsymbol{\sigma} \cdot grad(U)) + div(\boldsymbol{\sigma} \cdot (\vec{v} \times \vec{B})) \right) = 0 \qquad (28)$$

This equation used for definition of potential. Drop of potential inside Lithium defined by finite resistivity $\boldsymbol{\sigma} \cong 0.3 \cdot 10^7 [Ohm^{-1} m^{-1}]$.

Equations (1)-(3) correctly describe diffusion of filed inside Lithium. For example, substitute in (3) expression for current (1) one can obtain

$$div(grad(A_x)) + \mu \cdot j_x = div(grad(A_x)) - \mu \cdot \sigma \frac{\partial A_x}{\partial t} - \mu \cdot \sigma \cdot \frac{\partial U}{\partial x} + \mu \cdot \sigma \cdot (\vec{v} \times \vec{B})_x = 0, \qquad (29)$$

and so on for other components. It is clearly seen from here that this is diffusion (parabolic) equation with skin layer depth defined as characteristics of this equation, i.e.

$$\frac{1}{\boldsymbol{\delta}_e^2} \cong \frac{\mu \boldsymbol{\sigma}}{\tau} \qquad (30)$$

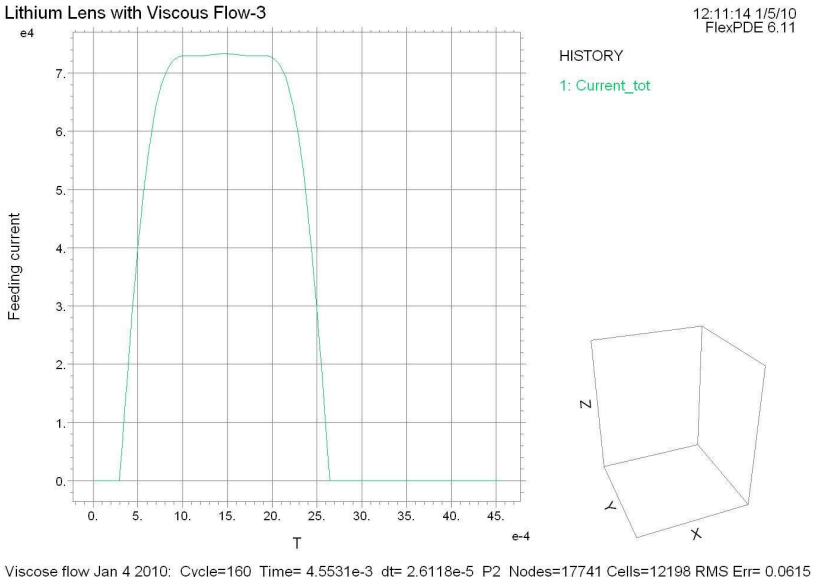

Figure 9: Electric current, *Ampers*.

Voltage applied to the lens taken as a sum of three odd harmonics

$$U(t) = U_0 \cdot [-4.5 \cdot Sin(\frac{\pi \cdot (t - \tau/10)}{\tau}) - 0.9 \cdot Sin(\frac{3\pi \cdot (t - \tau/10)}{\tau}) - 0.17 \cdot Sin(\frac{5\pi \cdot (t - \tau/10)}{\tau})] \quad (31)$$

for $\frac{1}{10}\tau < t < \frac{11}{10}\tau$ where $\tau = 2.3m\sec$. Beginning of the voltage pulse shifted from the moment of modeling start t=0 by $\tau/10$. Graph of current $J(t) = \int j_z(\vec{r})dS$, where surface integral of longitudinal component of current density is taken across the flow in central part, is shown in Figure above. Field histories are shown in Figure below for radial displacements r= 0.25; 0.4; 0.5; 0.6; 0.7; 0.8; 0.9; 1.2 $\times r_l$ where $r_l = 0.55cm$ stands for the radius of Lithium rod in central cross section

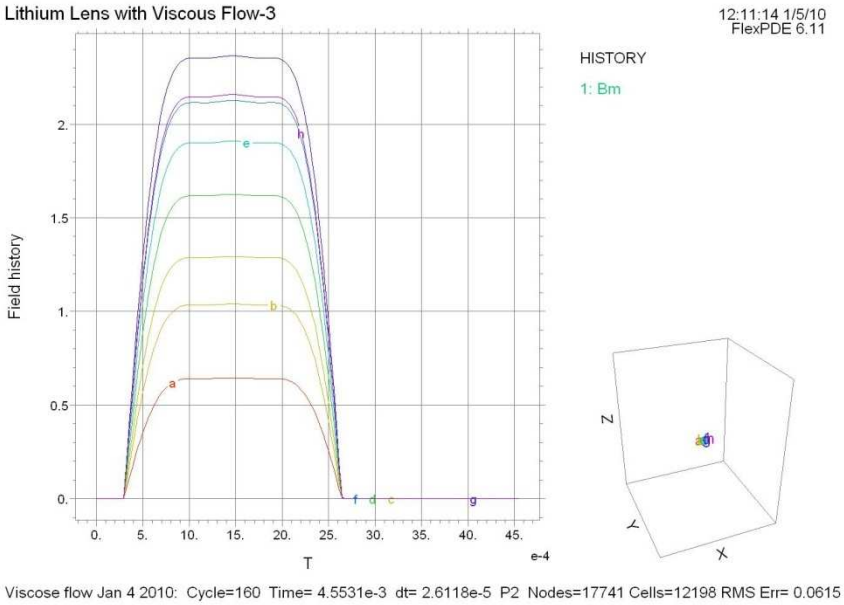

Figure 10: Magnetic field history for different radial positions. Diffusion terms turned "off". Field given in *Tesla* units.

Time scale in *seconds*, fields in *Tesla*. Maximal field value graph corresponds to displacement of 0.9 $r_l = 0.9 \times 0.55cm$. Terms in current ~ $-\sigma(\partial\vec{A}/\partial t)$ not included into this calculation.

The view of field with vector-potential terms, i.e. for $\vec{j} = \sigma\vec{E} = -\sigma(\partial\vec{A}/\partial t) - \sigma grad(U)$ represented in Figure below.

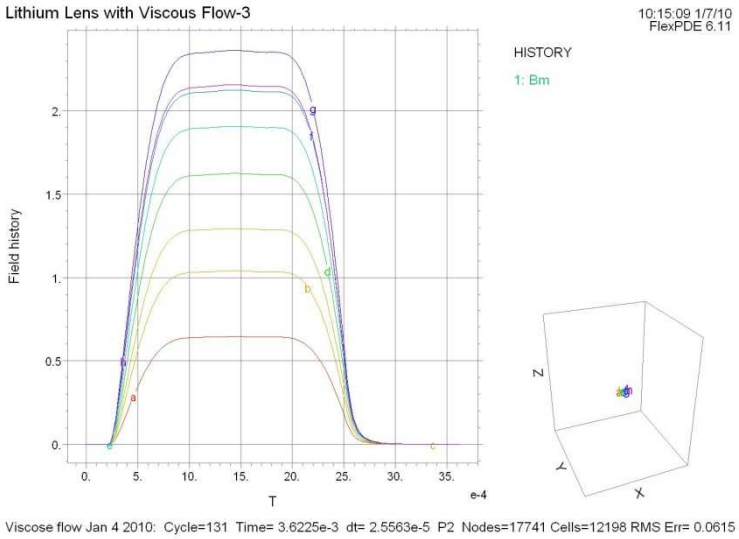

Figure 11: Magnetic field history with diffusion terms "on".

One can see, that the difference manifests in time regions, where variation of voltage rate is high (skin-layer build up and dissolving).

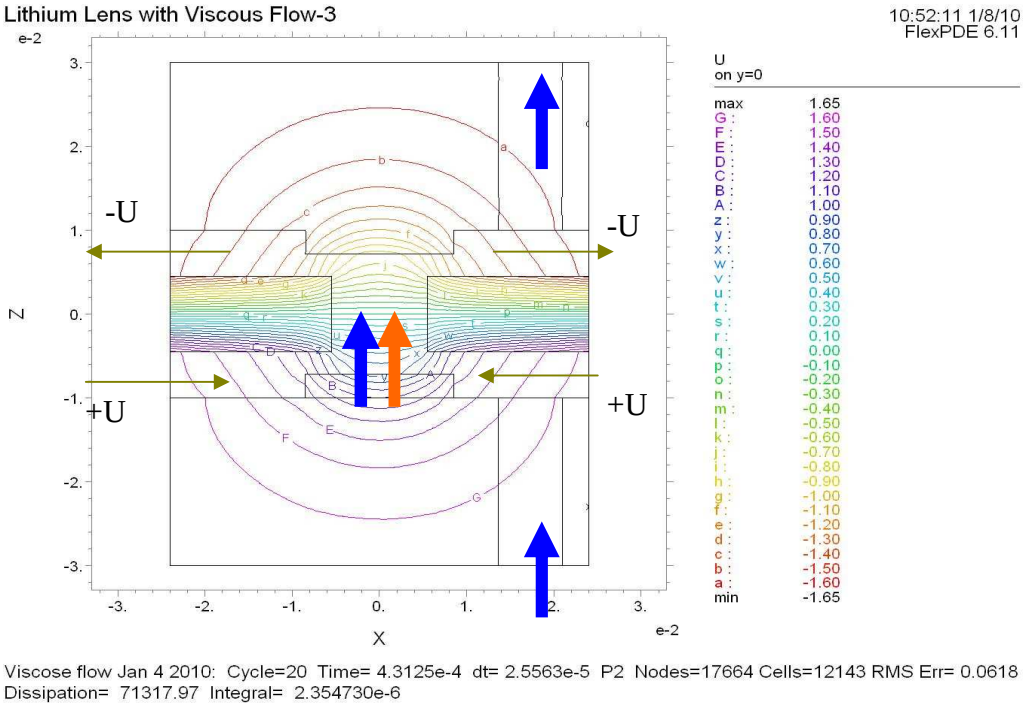

Figure 12: Potential. By blue arrows it is shown the Lithium flow, by red-current.

Voltage applied to the side surface of cylindrical boundary. In some runs we switched relative directions of current and liquid flow.

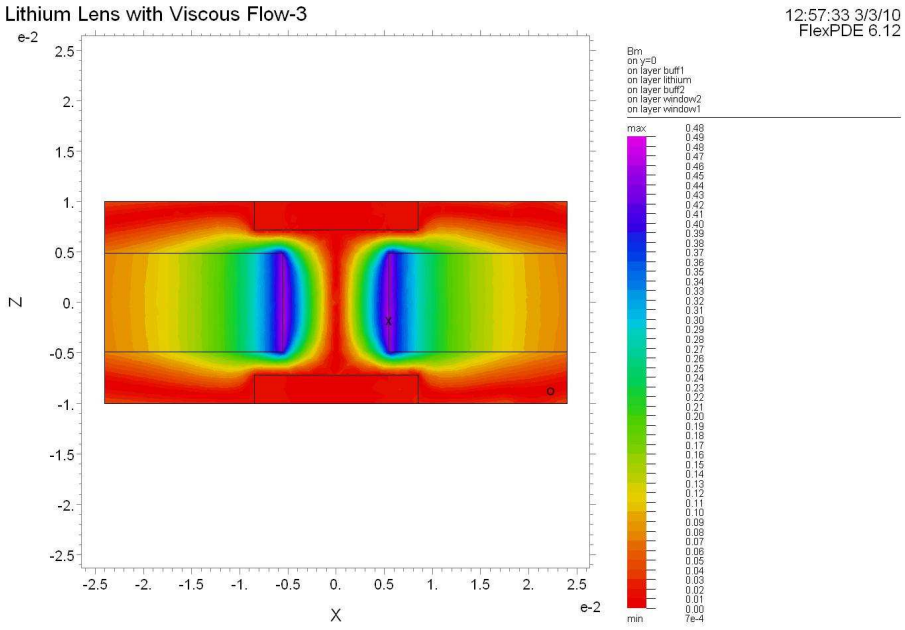

Figure 12: Magnetic field strength painted.

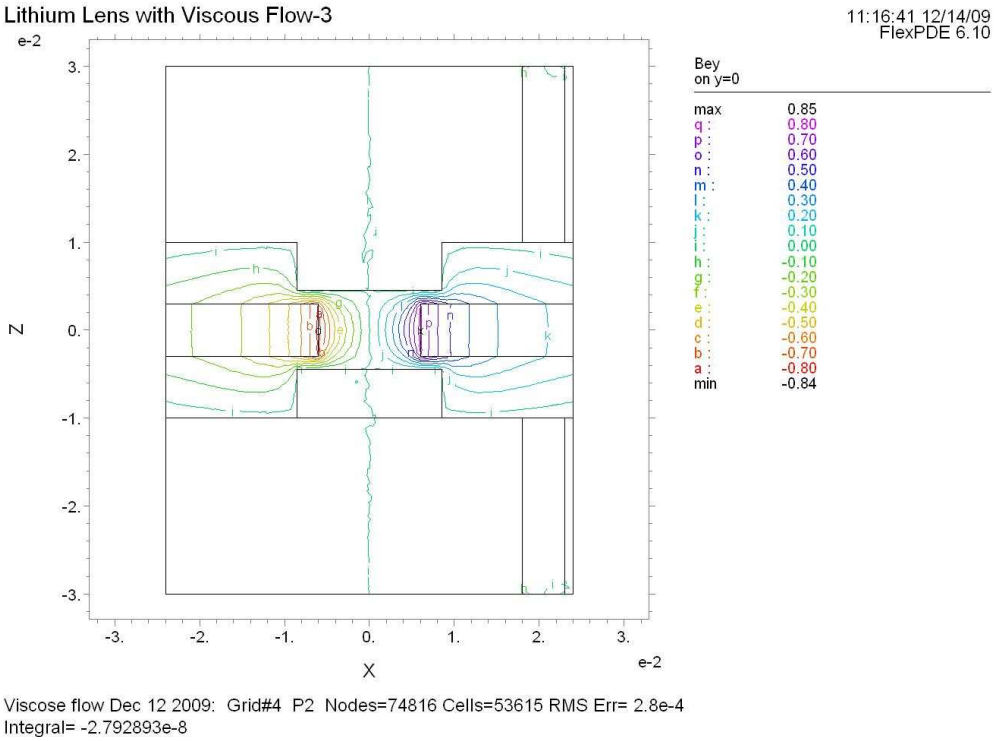

Figure 13: Vertical (longitudinal) magnetic field contours.

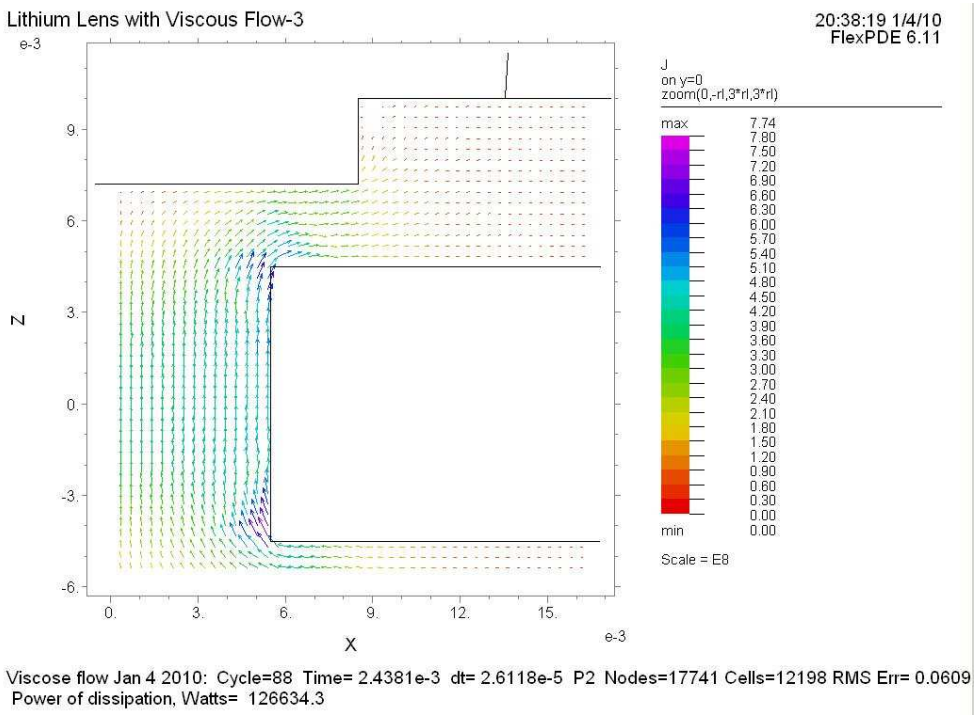

Figure 14: Vectors of current density. Value of current density represented by the length of arrows and theirs color.

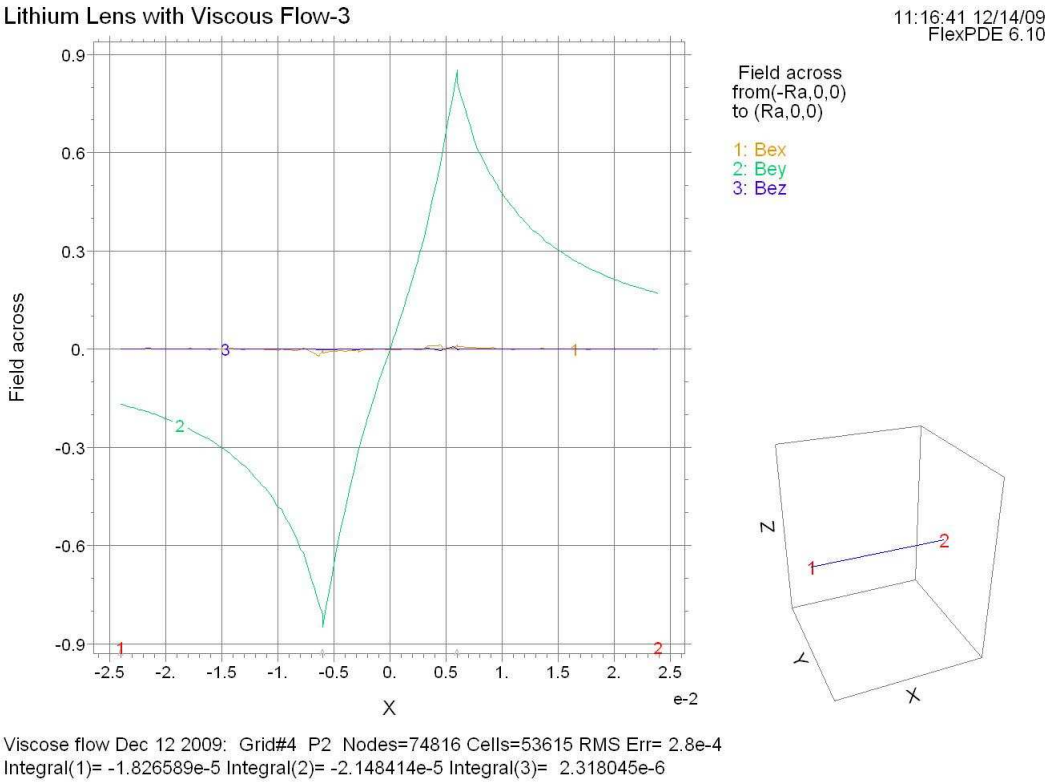

Figure 15: Field elevation across midplane of model.

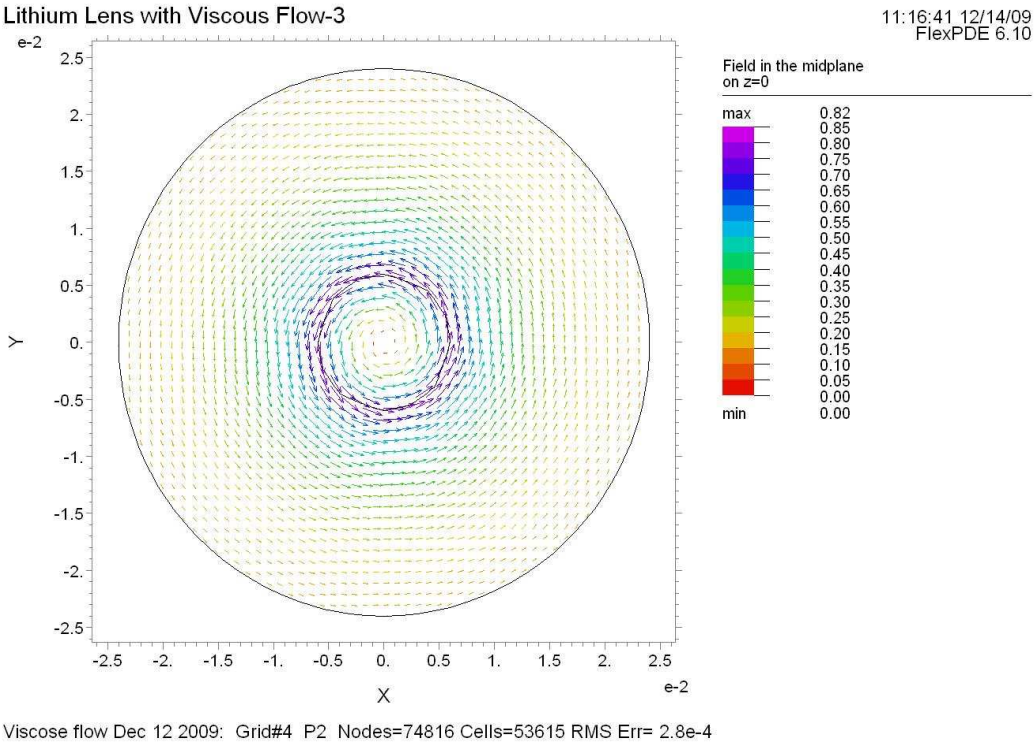

Figure 16: Magnetic vector field in midplane of model.

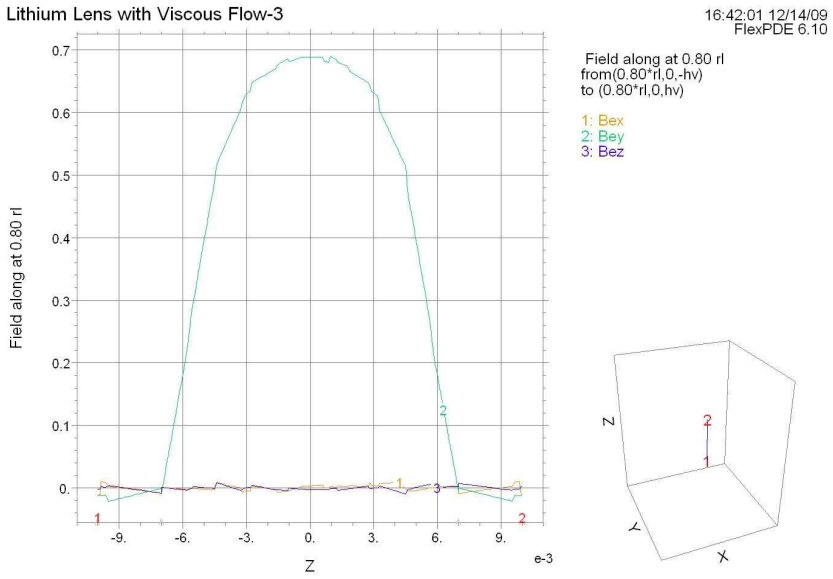

Figure 17: Longitudinal field dependence at 0.8 radius of lithium rod; $B(z) = B(x = 0.8r, y = 0, z)$

Family of graphs like in Fig. 17 for different offsets allow calculation of integral as function of transverse offset (displacement) , Figs. 18, 19. Namely,

$$Int(x) = \int_{-L}^{L} B(x, y = 0, z)dz$$

represented in Figs.18, 19 below.

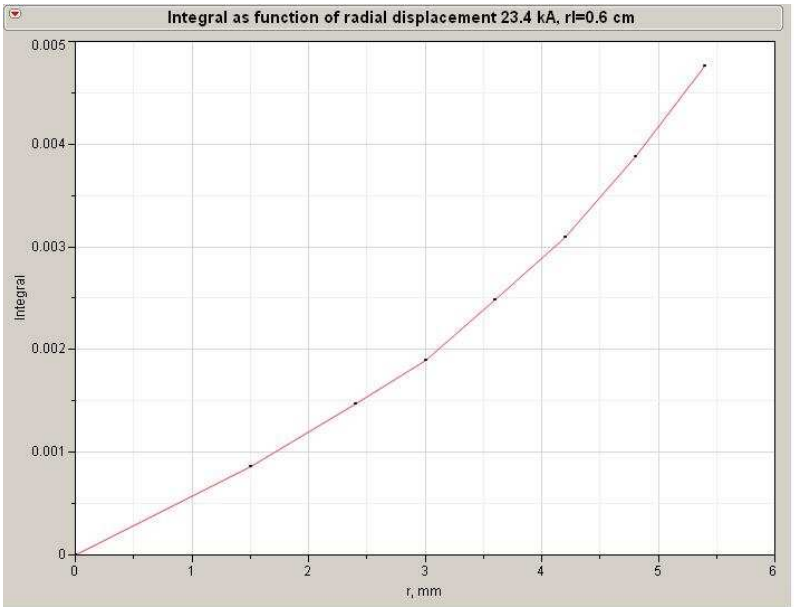

Figure 18: Field integral over longitudinal direction as function of radial displacement before correction of geometry made

Correction of geometry applied

Correction of Lithium flow radius, window radius were done while modeling.

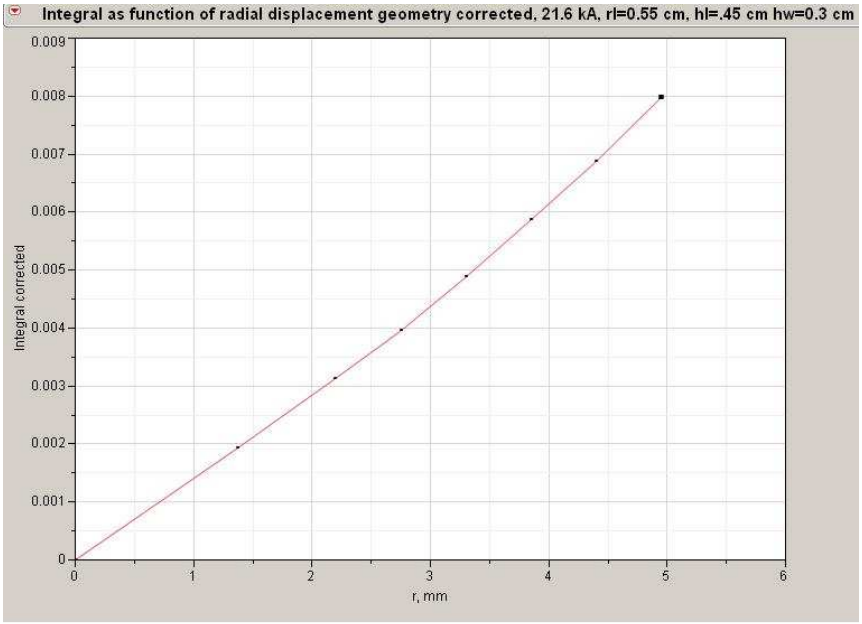

Figure 19: Field integral for corrected geometry

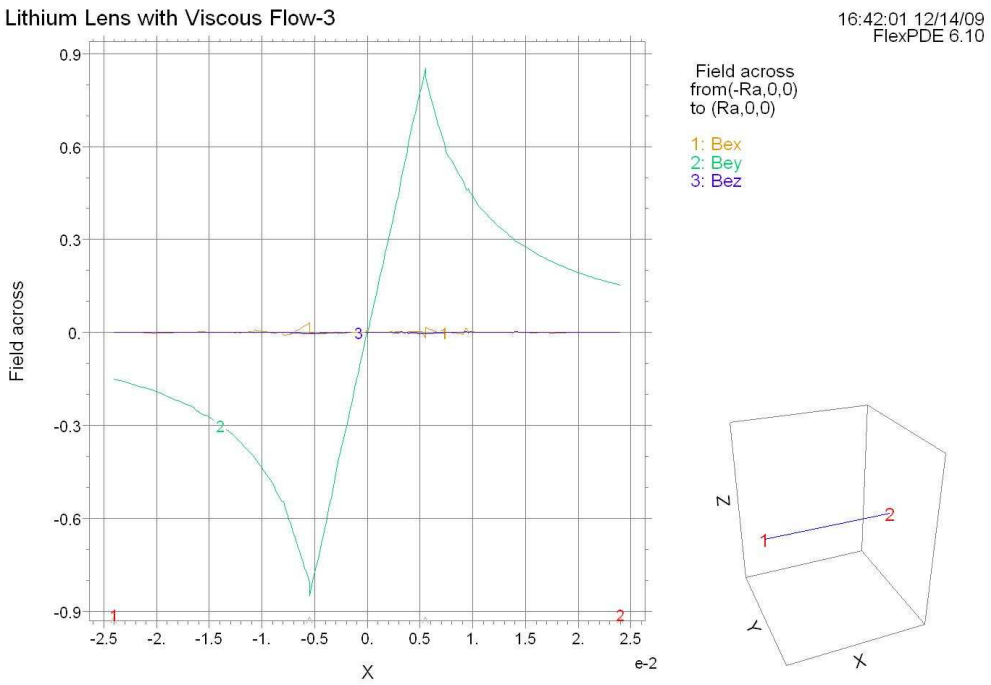

Figure 20: Field across. Corrected geometry

By comparing graphs in Fig. 20 - Fig.15 and Fig.18-Fig.19 one cans see, that the field dependence is much more linear after correction done.

LITHIUM FLOW

Flow of Lithium is governed by vector equation (7). In FlexPDE Grammatik components look like the following

vx: density*(dt(vx)+vx*dx(vx)+vy*dy(vx)+vz*dz(vx))+dx(p)-visc*div(grad(vx))= xcomp(cross(J,B))

vy: density*(dt(vy)+vx*dx(vy)+vy*dy(vy)+vz*dz(vy))+dy(p)-visc*div(grad(vy))= ycomp(cross(J,B))

vz: density*(dt(vz)+vx*dx(vz)+vy*dy(vz)+vz*dz(vz))+dz(p)-visc*div(grad(vz)) = zcomp(cross(J,B))

FlexPDE-version 6 allows writing this system as single vector equation

density*(dt(v)+dot(v,grad(v)))+grad(p)-visc*div(grad(v)) – $^1/_3$*visc*grad(div(v))=cross(J,B)

(compare with (13):

$$\rho\cdot\left(\frac{\partial\vec{v}}{\partial t} + (\vec{v}\cdot\vec{\nabla})\vec{v}\right) + grad(P) - \eta\cdot\nabla^2\vec{v} - \left(\zeta+\tfrac{1}{3}\eta\right)grad(div(\vec{v})) = (\vec{j}\times\vec{B}) \quad)$$

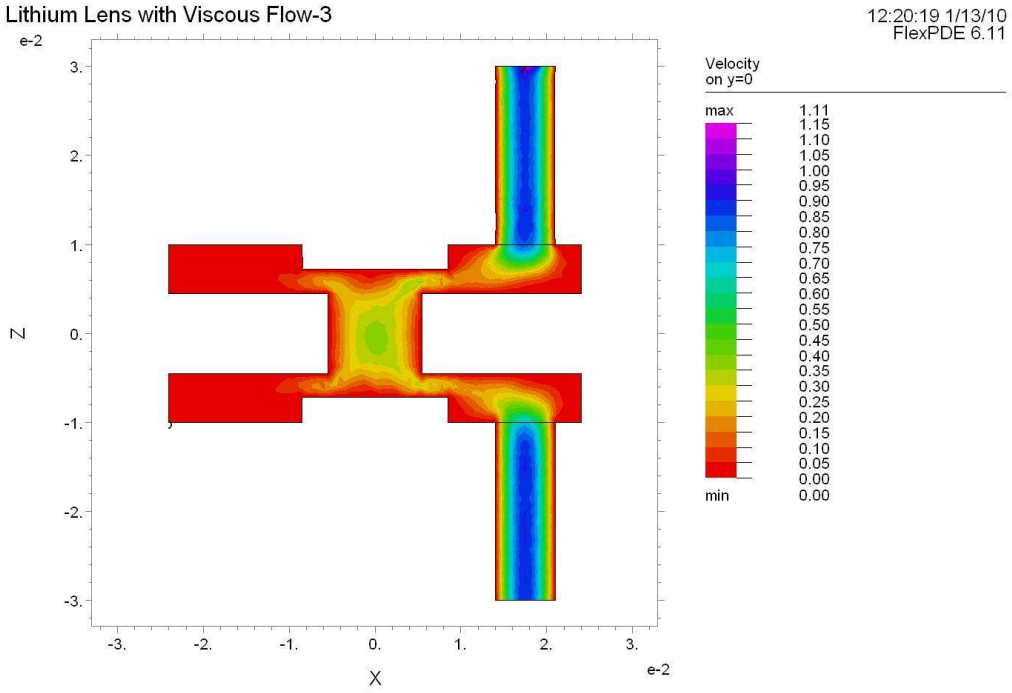

Figure 21: Contour of Lithium velocity module.

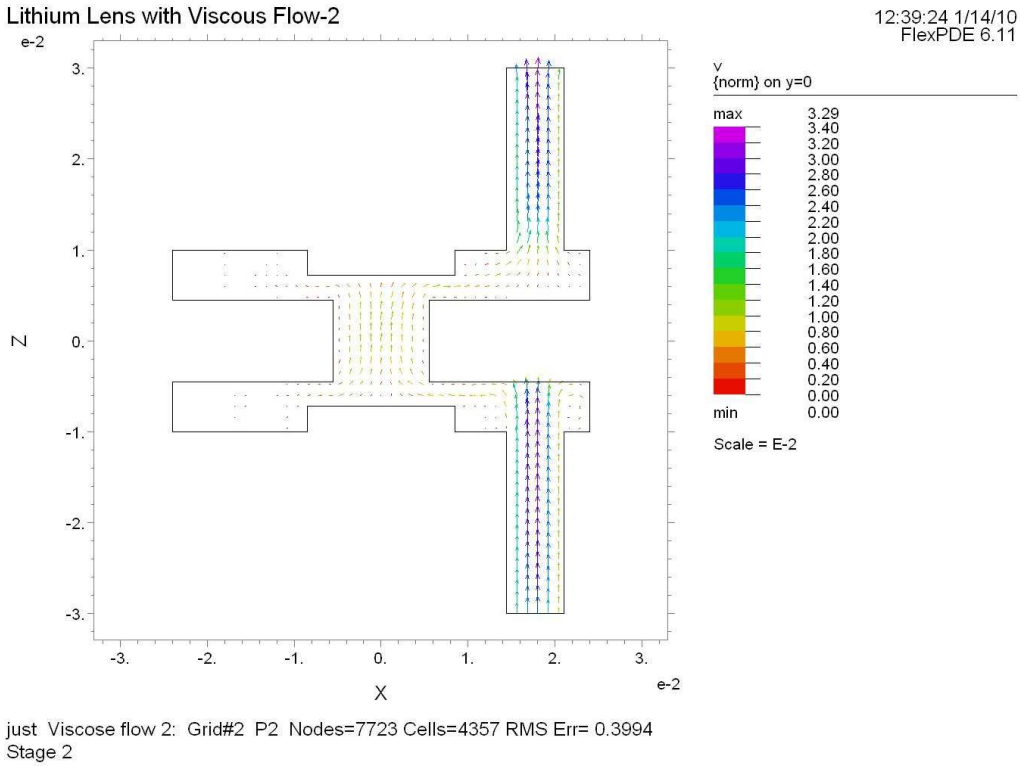

Figure 22: Vectors of velocity, no electrical current yet.

High pressure; stationary solution for $\vec{v} \perp \{x \times z\}$. Tubes have off set ~0.01mm. Re~2865.

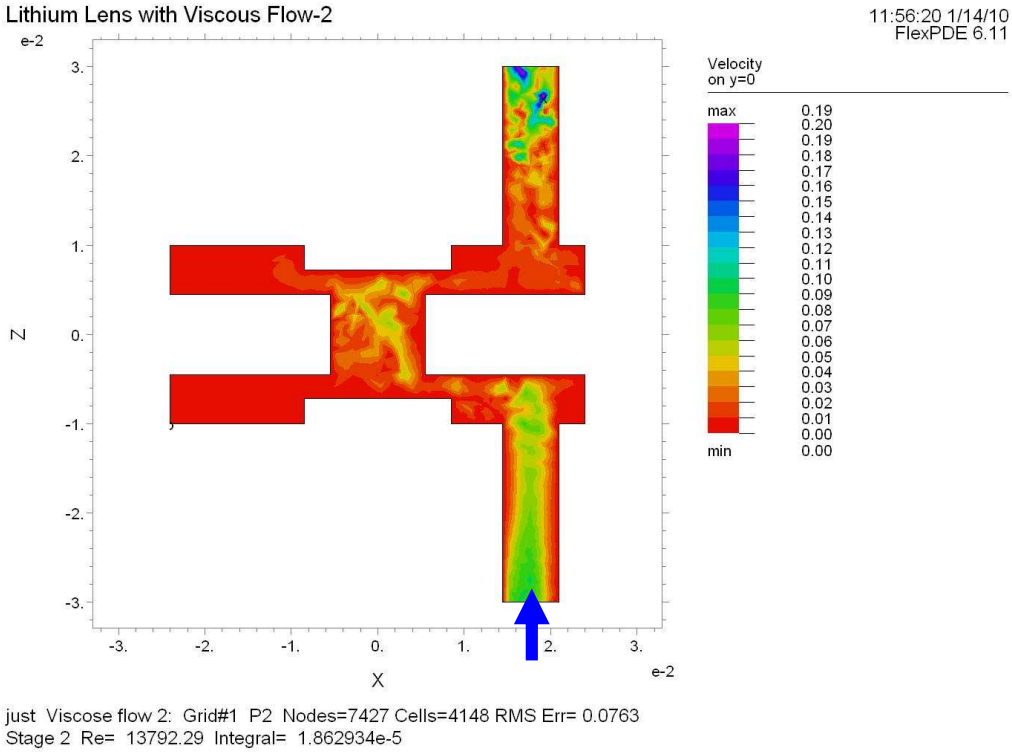

Figure 23: Developed turbulent flow at higher Reynolds number with different initial pressure and pressure drop along the Lithium flow during transition.

Despite the turbulence is pretty developed, the flow in central region remains quiet as is could be seen in Figure below.

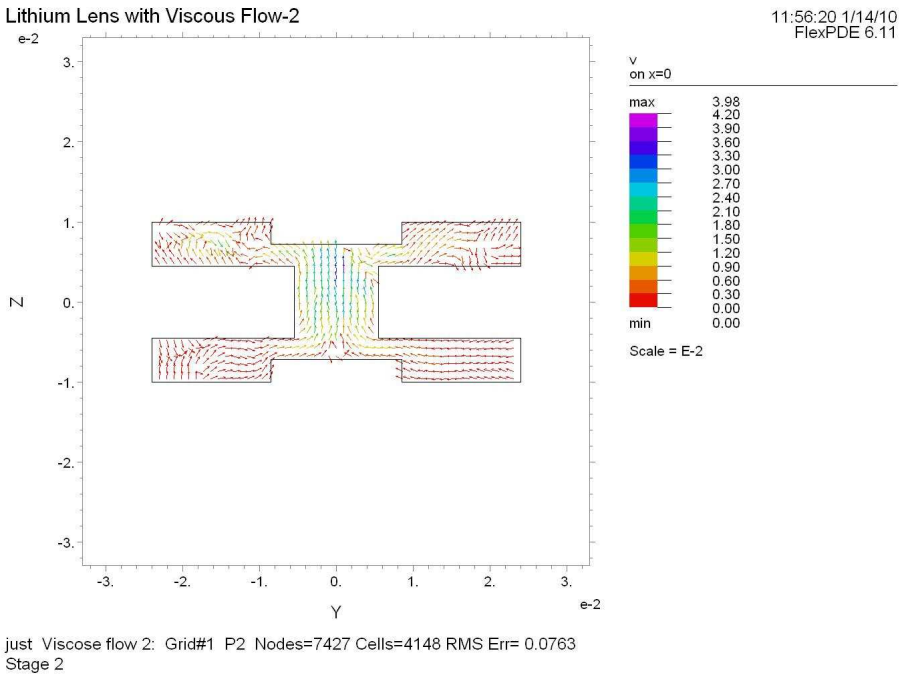

Figure 24: Velocity vector plot; by the cut made in orthogonal plane.

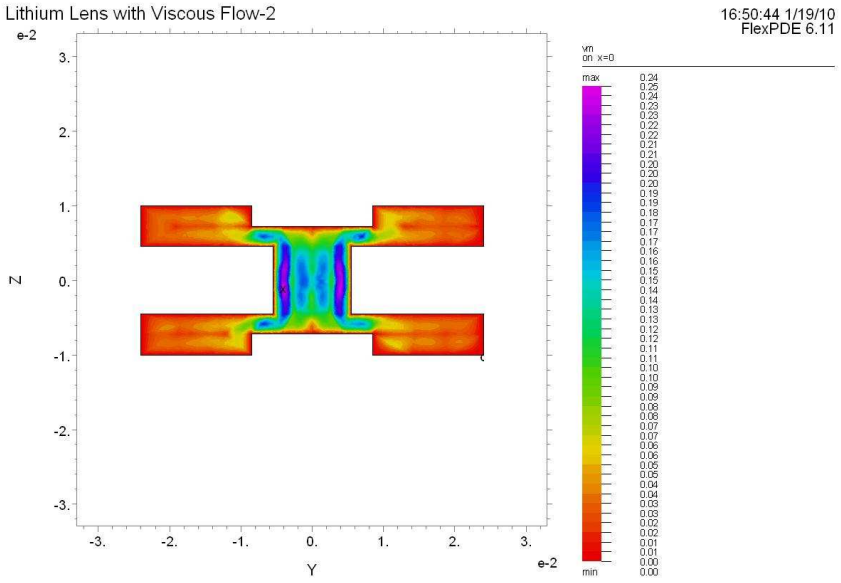

Figure 25: The same cut as in previous figure, but now the $v_m = \sqrt{v_x^2 + v_y^2 + v_z^2}$ is painted by color.

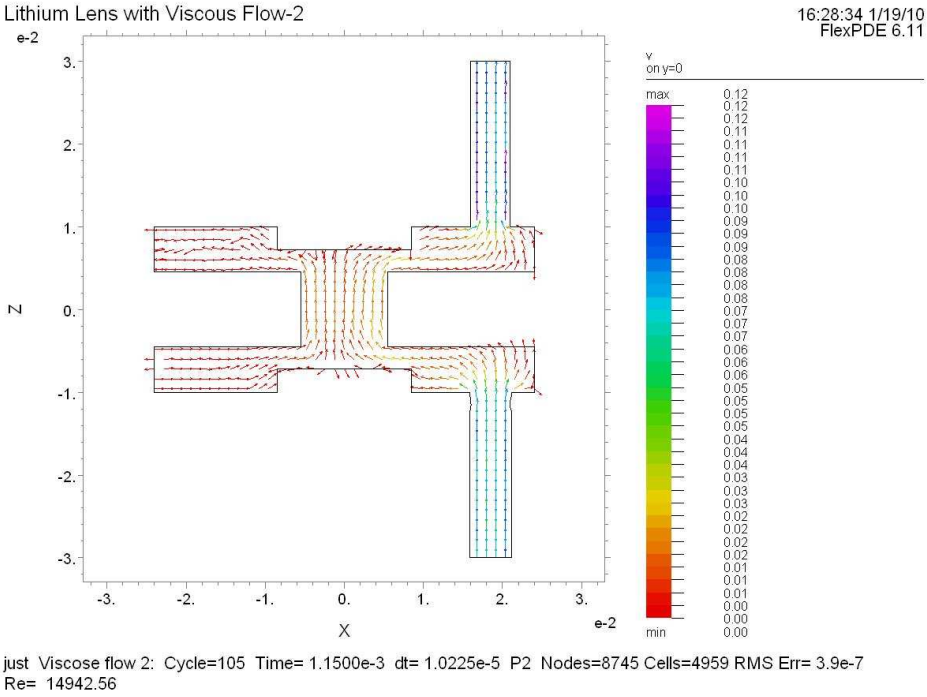

Figure 26: Re~15000; time dependent problem with linear pressure drop rise. One can see, that central axis of flow is shifted. Arrows normalized to the same length; velocity represented by color.

As we could expect from equation (12) the pressure gradient developed by term $(\vec{j} \times \vec{B})$ is big in comparison with pressure drop along lithium flow (between inlet and outlet orifices).

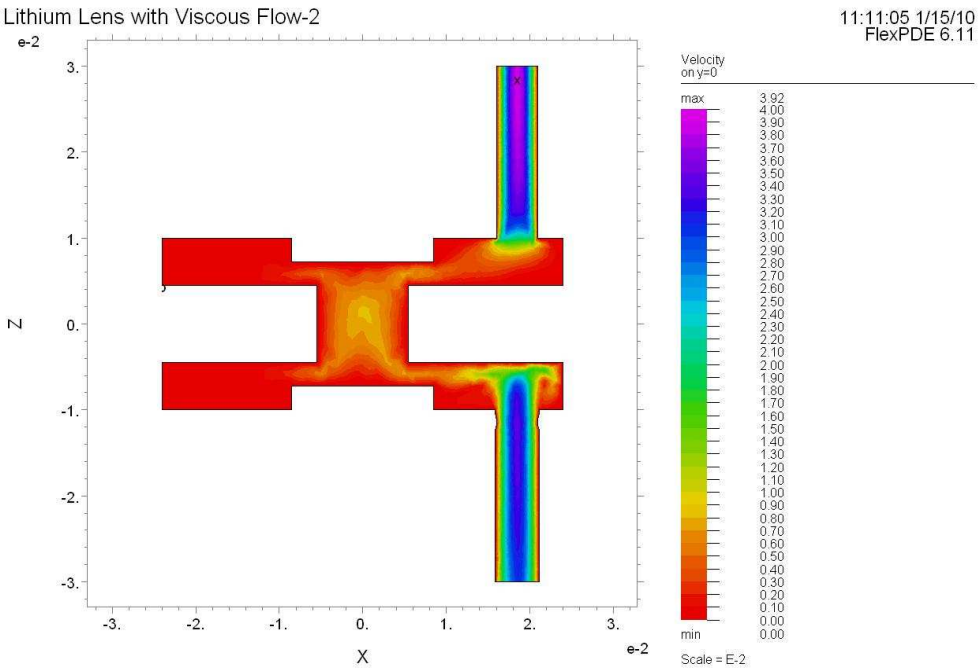

Figure 27: Inlet tubes slightly squeezed.

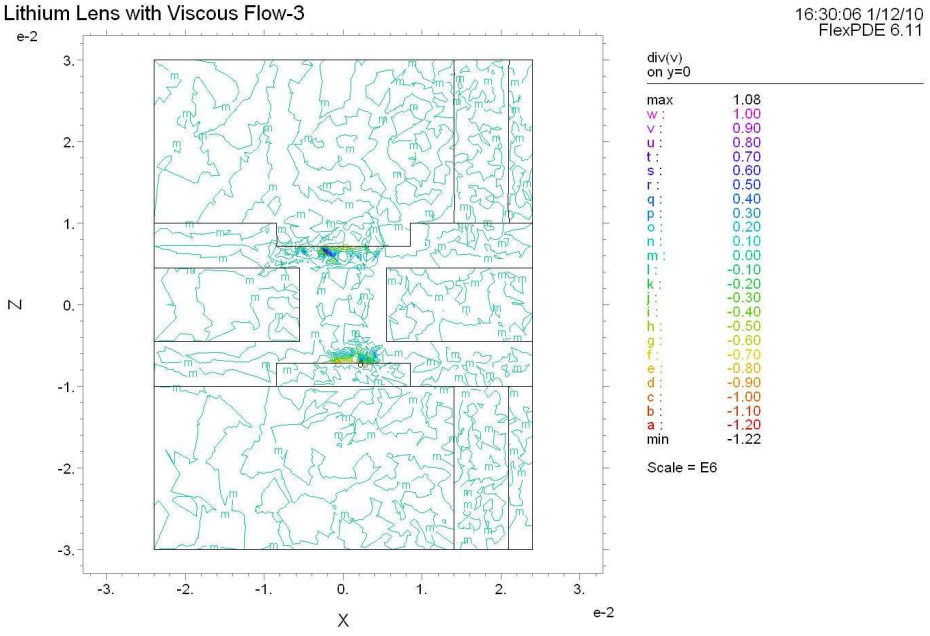

Figure 28: Contour plot of $div(\vec{v})$; it is zero practically everywhere with numeric accuracy.

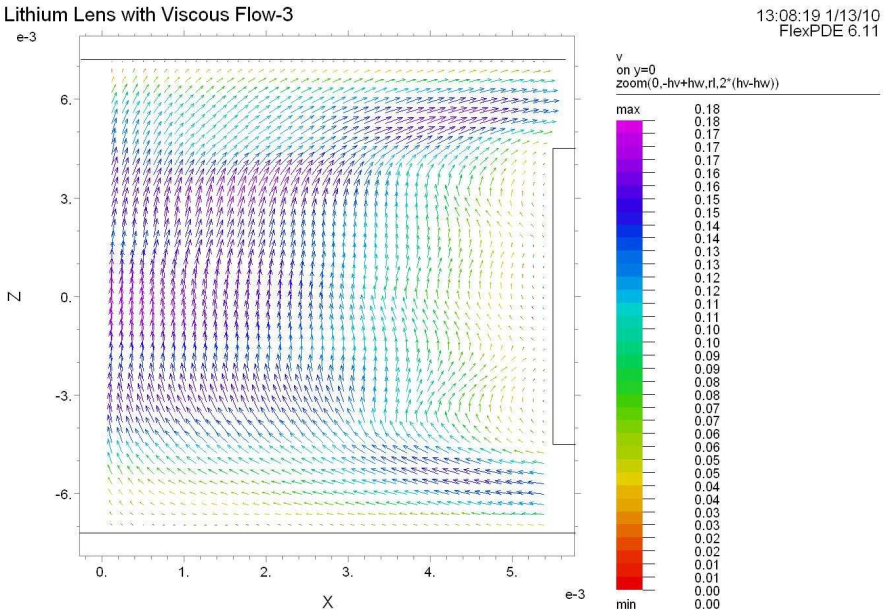

Figure 29: Vectors of velocity zoomed. Left axis coincides with lens axis.

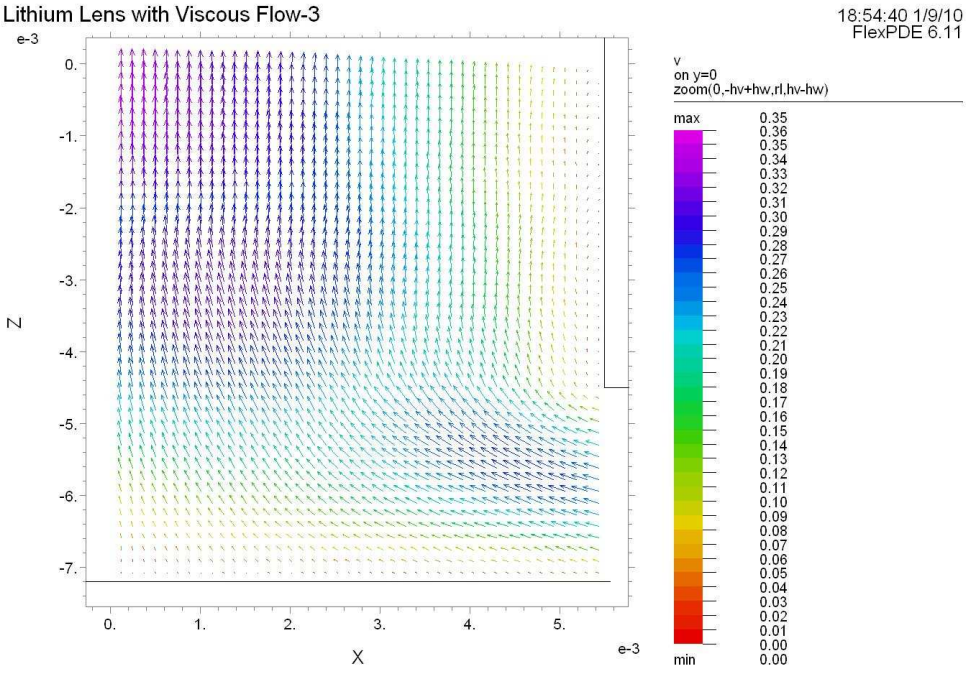

Figure 30: Velocity profile from previous Figure zoomed; no electric current.

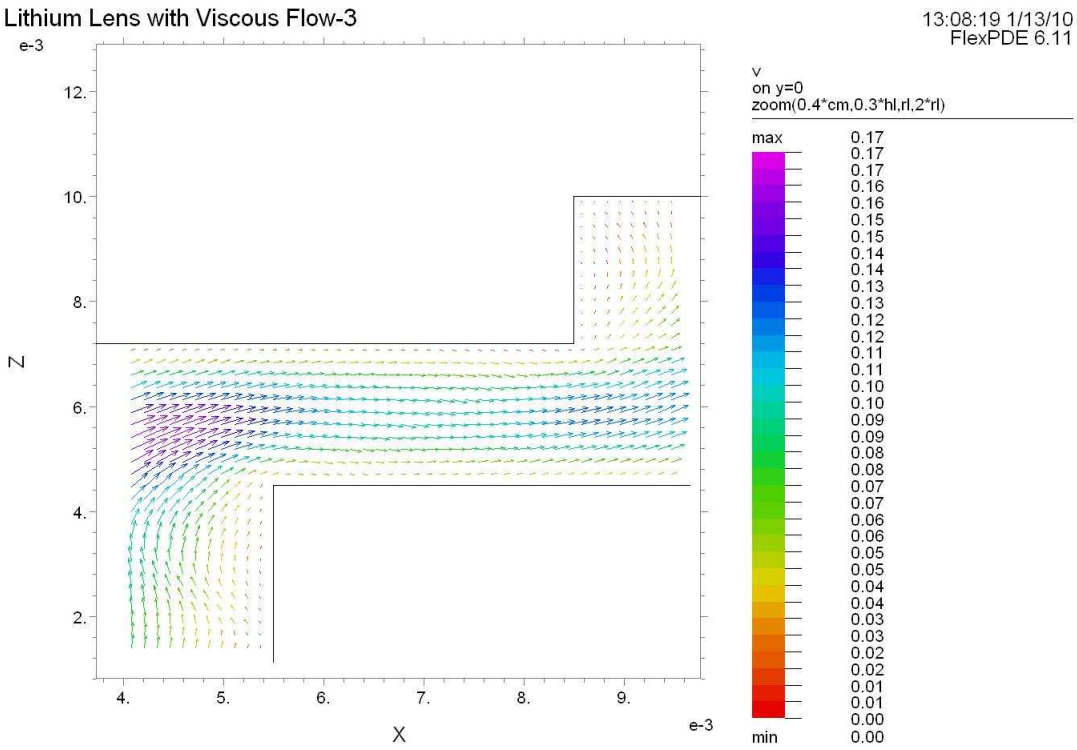

Viscose flow Jan 12 2010: Cycle=2 Time= 5.7500e-5 dt= 2.8750e-5 P2 Nodes=18469 Cells=12705 RMS Err= 0.0427
Reynolds number max= 34173.52

Figure 31: Vectors of Lithium flow in transition volume.

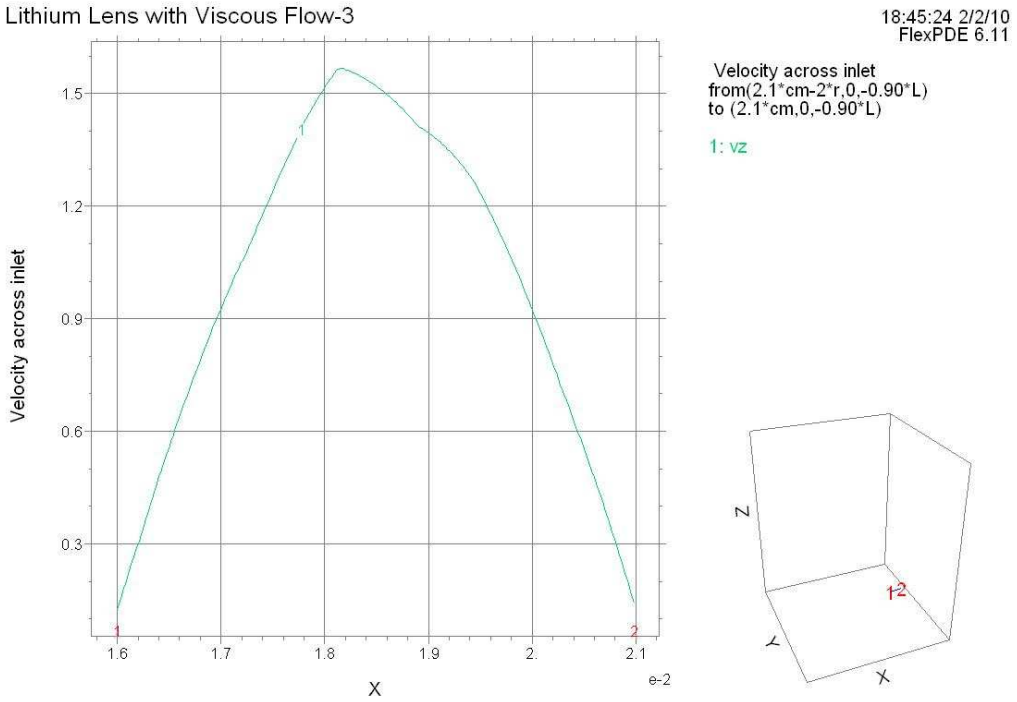

Viscose flow Feb 2 2010: Cycle=236 Time= 2.6565e-3 dt= 1.0225e-5 P2 Nodes=78853 Cells=56472 RMS Err= 0.0428
Reynolds number max= 27266.31 Integral= 5.033945e-3

Figure 32: Velocity profile across inlet tube. Some deflection of profile from parabolic defined by accuracy of calculation.

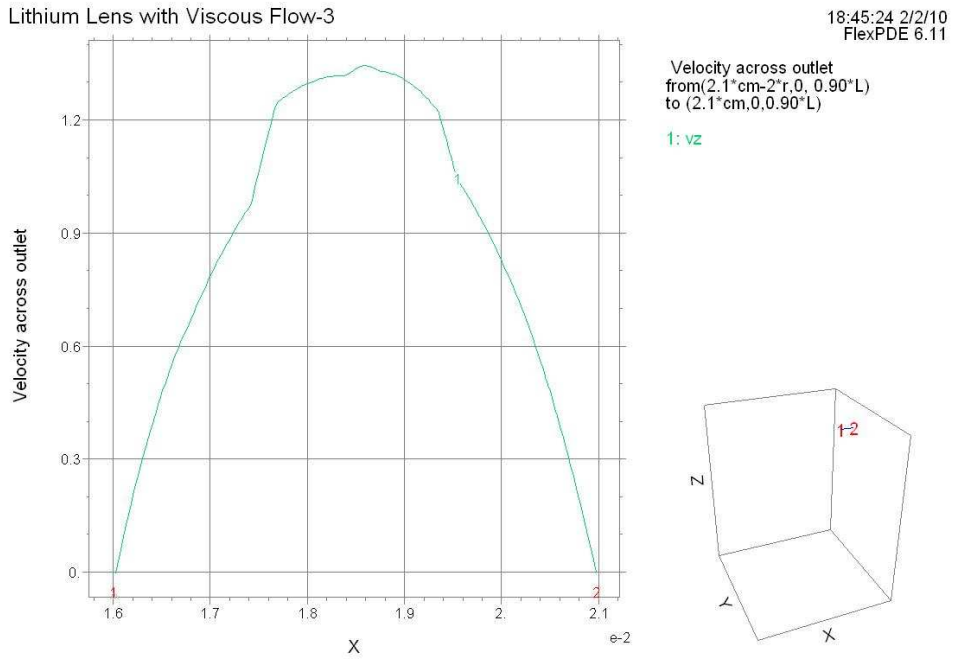

Figure 33: Velocity profile across outlet tube.

One can see that the velocity profiles are the same at input and output tubes.

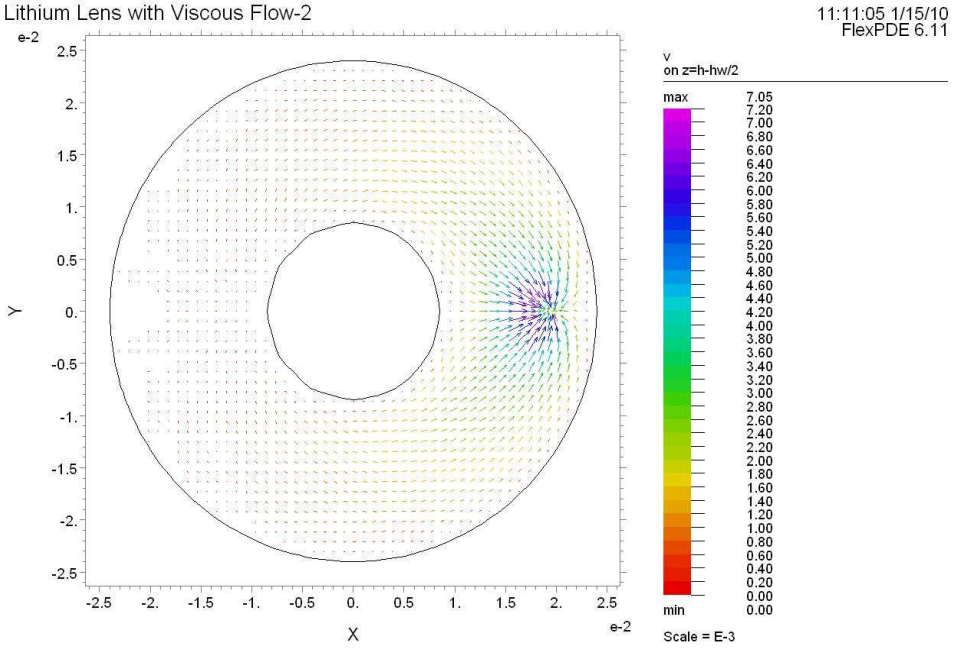

Figure 34: Velocity profile just below outlet tube.

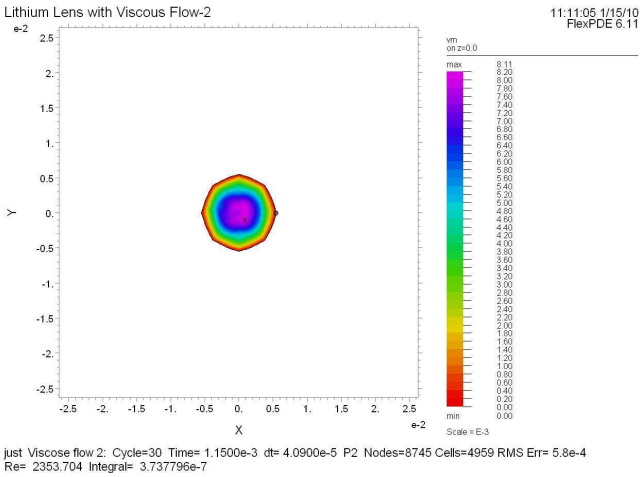

Figure 35: Velocity profile in the middle of model (across the plane with central point {x=0, y=0, z=0}.

Now the current is running; Figures below reflect circulation forced by $\vec{J} \times \vec{B}$ term.

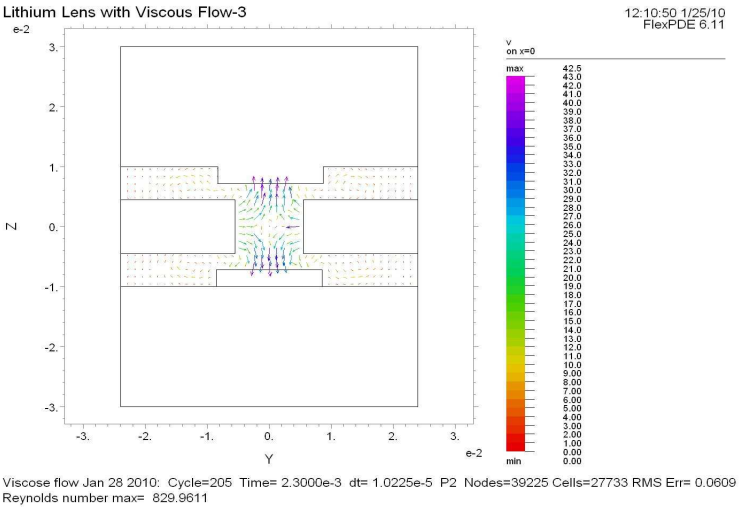

Figure 36: Velocity vector-field. Term with $\vec{J} \times \vec{B}$ is now included; maximal field.

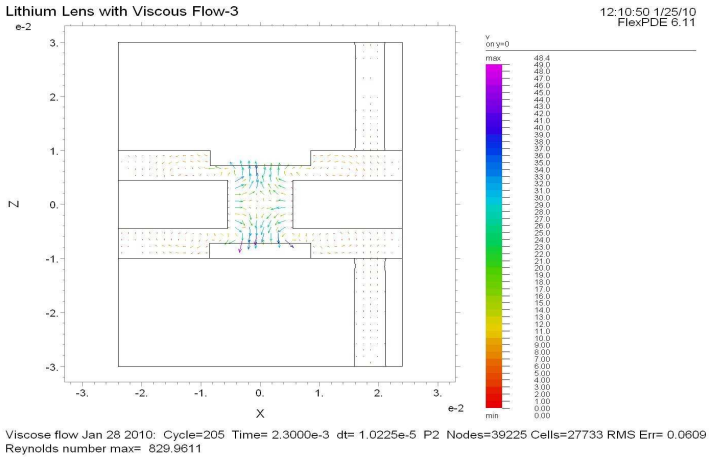

Figure 37: Cut in rectangular plane.

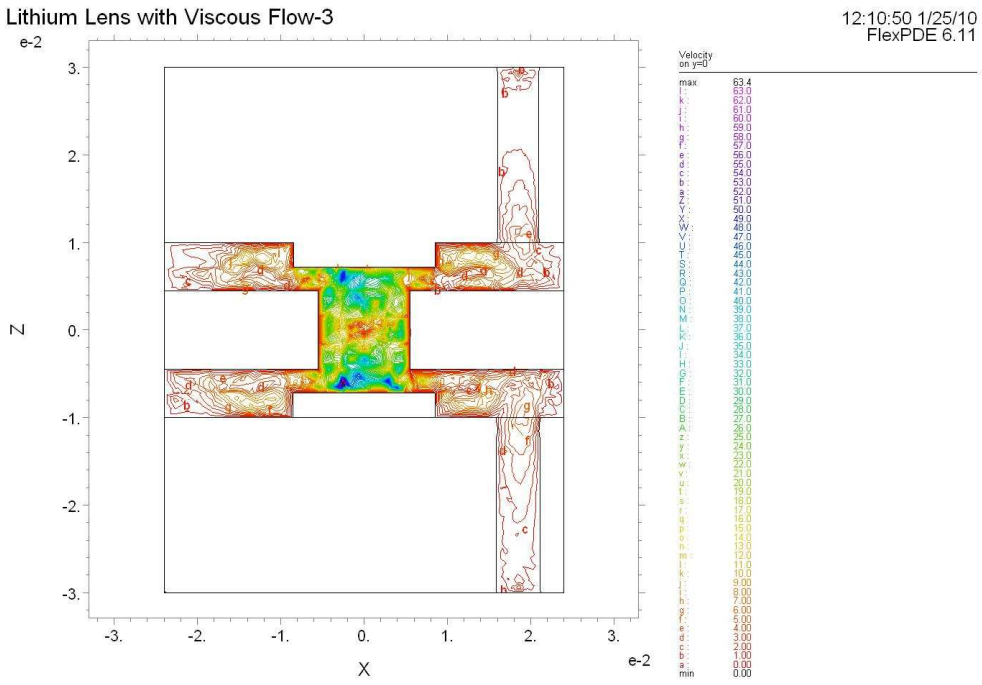

Figure 38: Velocity contours joint points with the same velocity module.

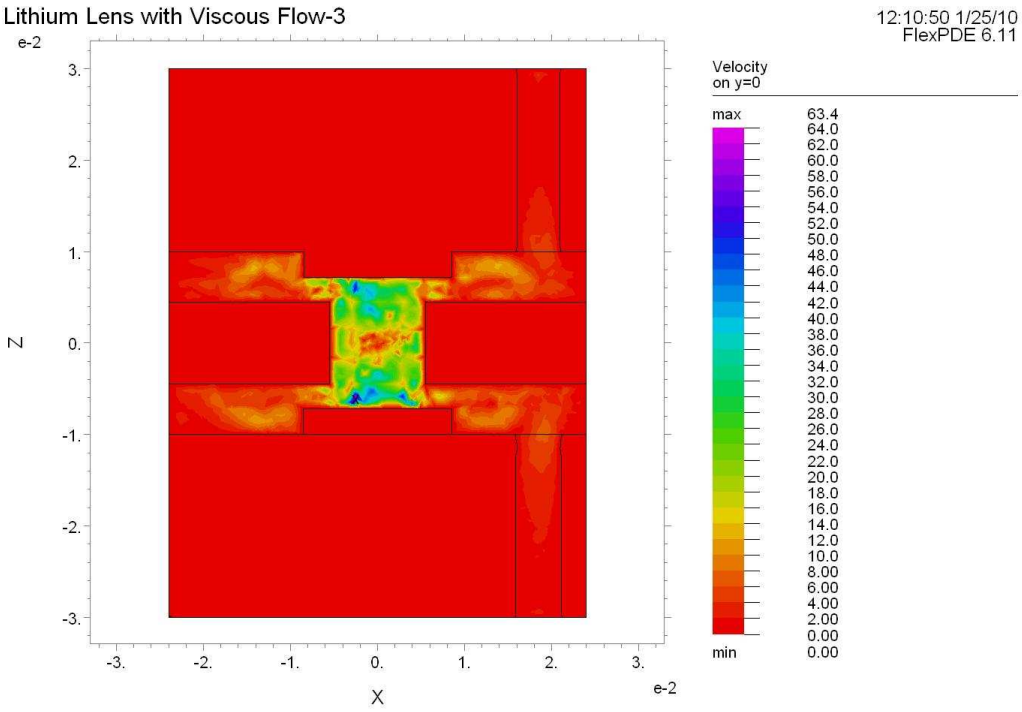

Figure 39: Velocity contour painted. One can see asymmetry induced by systematic flow. Turbulence pretty manifested.

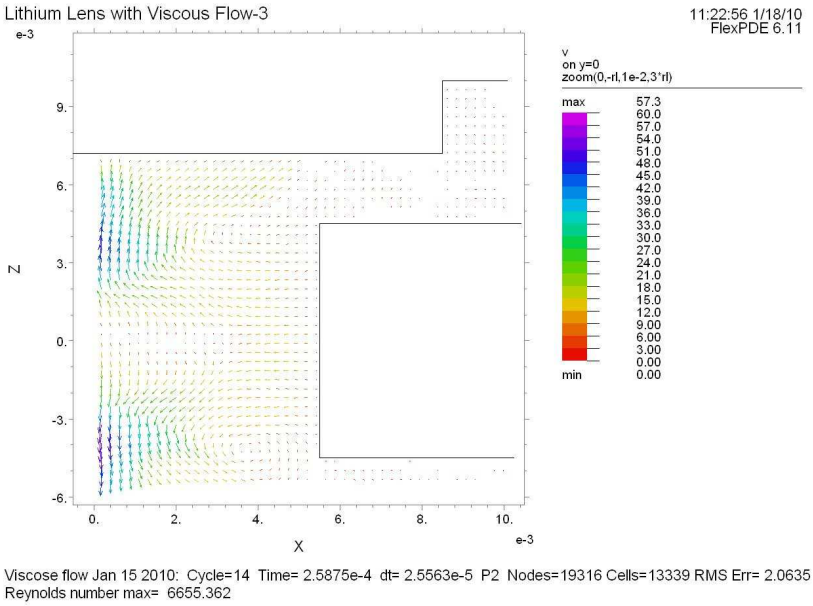

Figure 40: Plot of velocity (Fig.37) zoomed. Left side coincides with axis of lens. Circulation is clearly seen here. Moments of time correspond to the field at maximum.

Typical dependences of Re number during rise of pressure drop to its maximal value **delp**=1N/m^2 according to the low

p_in=1e6

p_out= IF t<tau/10 THEN p_in-delp*10*(t/tau) else p_in-delp

is shown in Fig below.

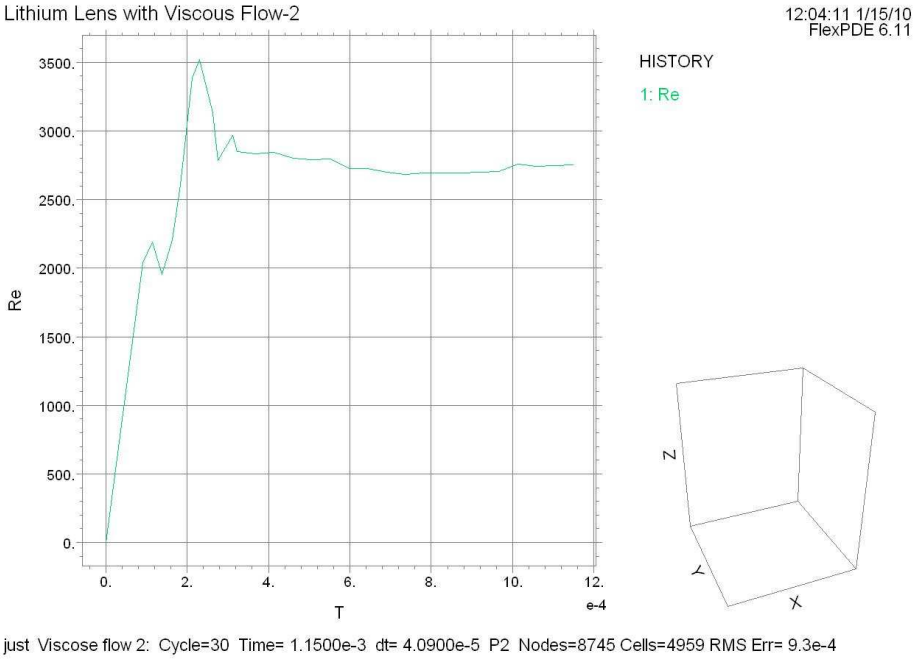

Figure 41: Time variations of Reynolds number while the change of pressure drop.

Would like to attract attention, that viscosity is so small (in numerical expression), so the pressure drop along the model is very small.

TEMPERATURE

One can see that equation (19) is a parabolic (diffusion) type. Really, the temperature relaxation in absence of dissipation (after feeding pulse is gone), time dependence of temperature defined by (19) with all terms at right side set to be zero, divergence also, so

$$\rho \cdot C_p \left(\frac{\partial T}{\partial t} + \vec{v} \cdot grad(T) \right) - div(k \cdot grad(T)) + P \cdot div(\vec{v}) = (\vec{j} \cdot \vec{E}) + \sigma'_{ik} \frac{\partial v_i}{\partial x_k} + \dot{Q}(\vec{r}, t)$$

comes to

$$\rho \cdot C_p \cdot \left(\frac{\partial T}{\partial t} + \vec{v} \cdot grad(T) \right) - div(k \cdot grad(T)) = 0 \quad . \tag{32}$$

As we already mentioned, (26), thermal skin layer $\boldsymbol{\delta_T}$ defined by characteristic of this equation as

$$\frac{k}{\boldsymbol{\delta_T^2}} = \frac{\boldsymbol{\rho} C_p}{\boldsymbol{\tau}} \quad , \tag{33}$$

and it makes diffusion processes mentionable here.

Initial profile of temperature was set as **Temp = Ta+(Tb-Ta)*(z+L)/2/L** as a start one; it is quickly reversed to proper one. In case, when temperature of lens boundaries kept constant, temperature was set as **Temp=Ta** at all boundaries

The source of heating in equation (19), $(\vec{j} \cdot \vec{E})$ represented in Fig. 42 below.

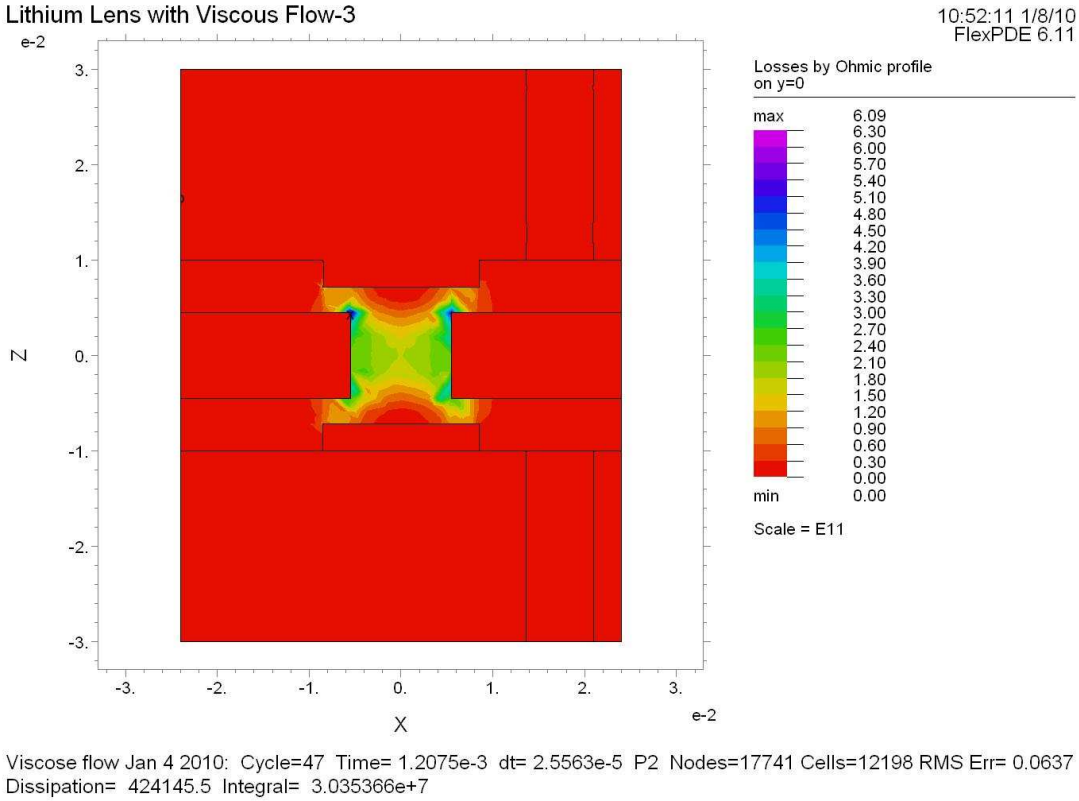

Figure 42: Ohmic losses.

Viscous losses calculated with formula (6) represented in Fig. 43 below.

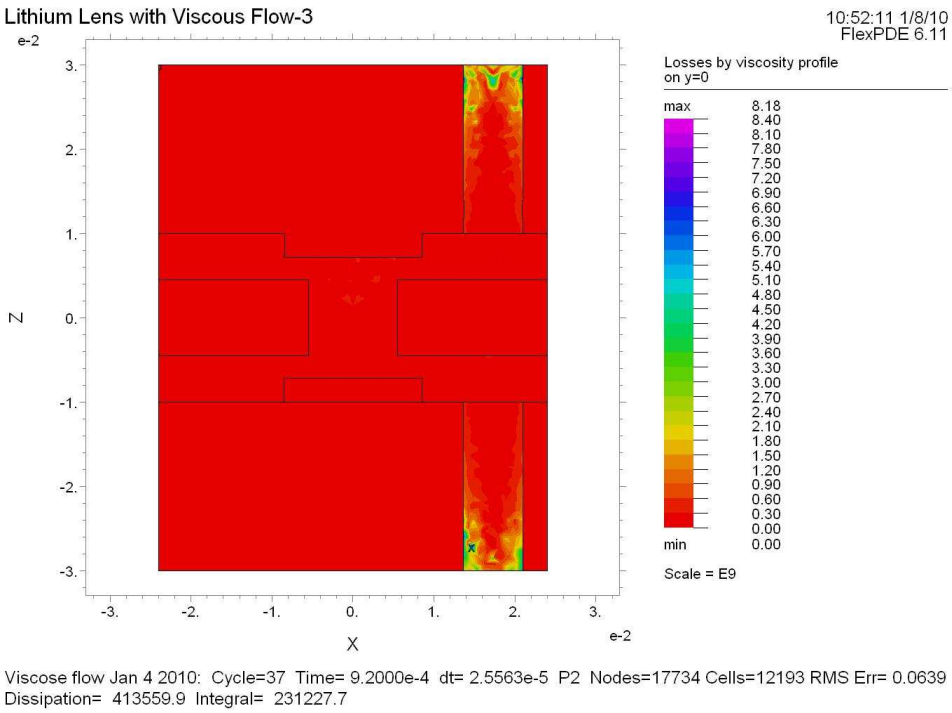

Figure 43: Viscose losses, formula (22).

One can see, that these losses manifest in transition region. We would like to attract attention that scales in Figs differ 1000 times.

Temperature history calculated for few scenarios. In a first one the fixed temperature kept at the entrance and exit only allowing establishing temperature at the walls in between by the heat generation.

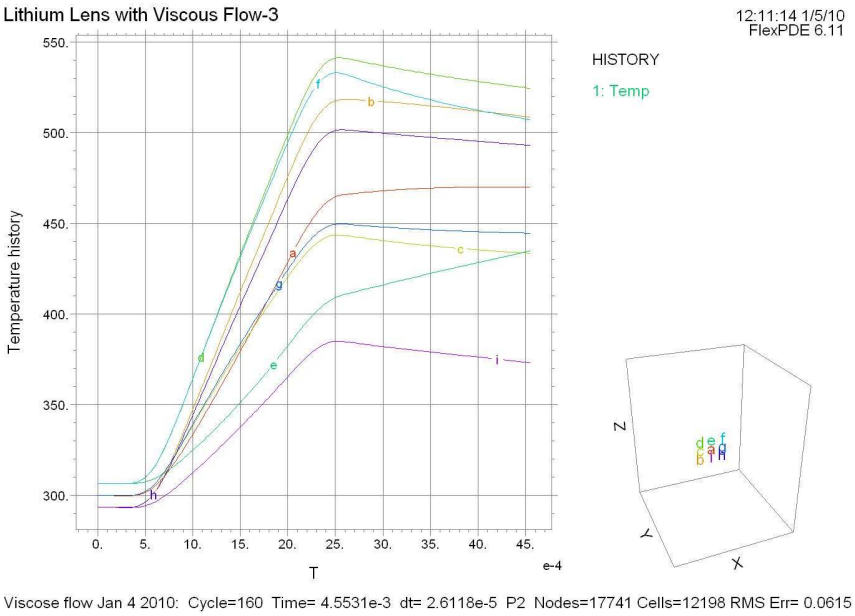

Figure 44: Temperature history for six different positions.

Locations of points where temperature represented shown in Fig.45 below

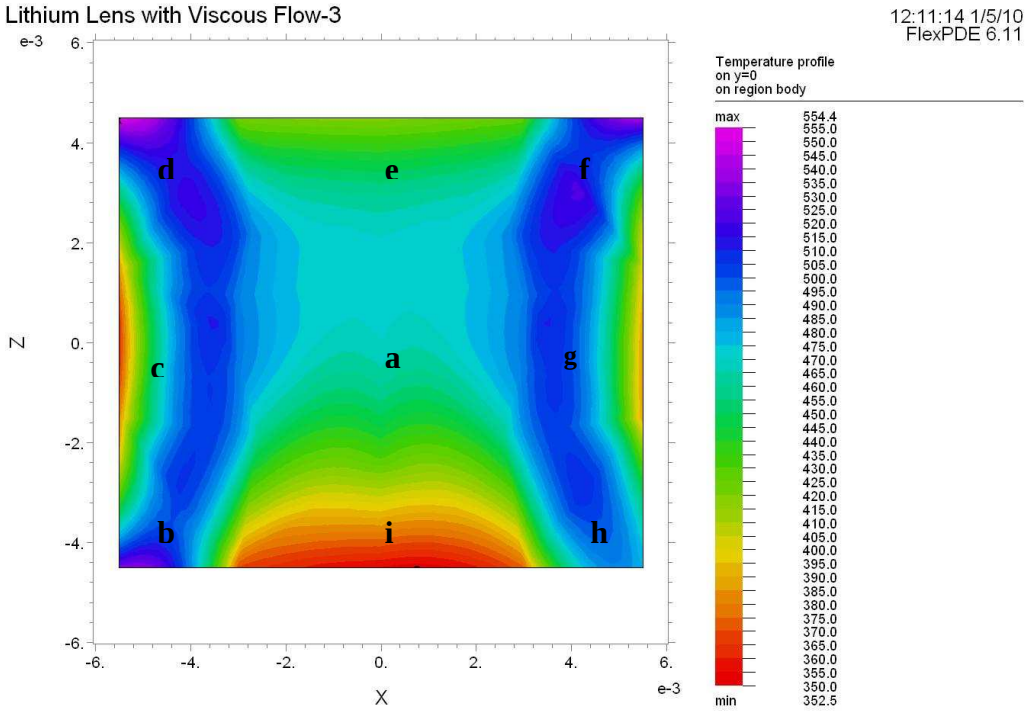

Figure 45: Temperature profile painted. Letters correspond to the graphs in previous Figure 44. Points **f** and **h** located at the side with outlet and inlet tubes respectively.

Next Figures show the temperature and its profile at ~12msec.

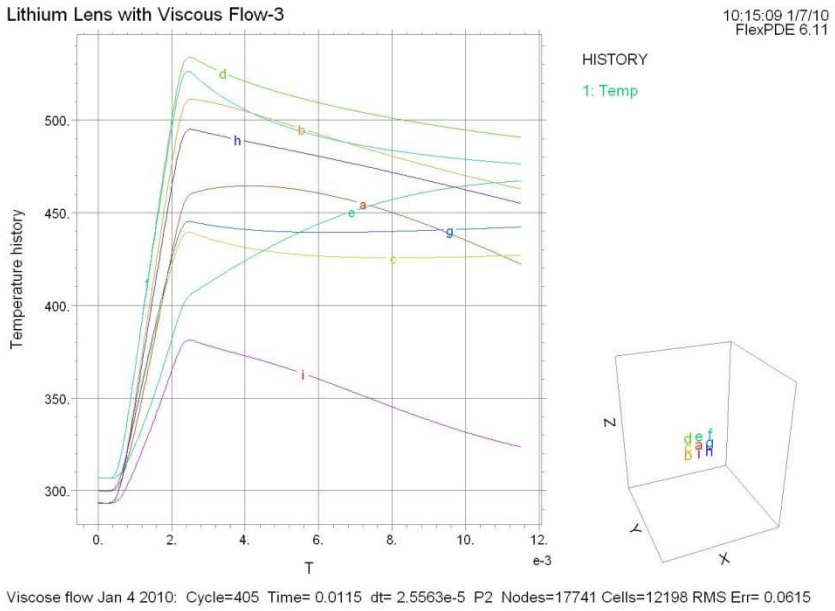

Figure 46: Temperature graph extended to ~12 *msec*. Points are the same as in previous Figure.

Temperature rise at point ***e*** (and ***g***) is a result of drift more warmer pats of liquid towards the outlet tube.

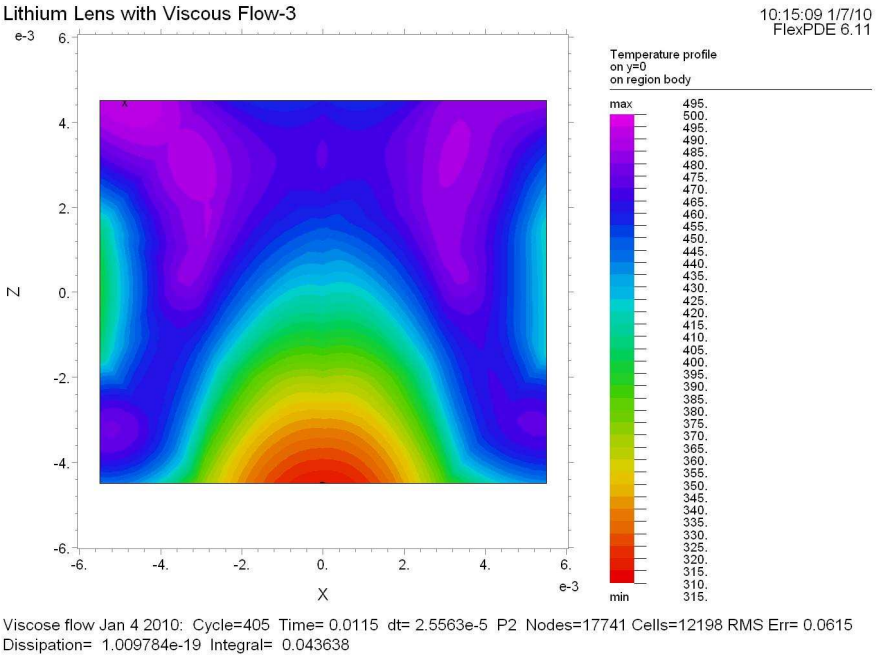

Figure 47: Temperature profile painted, 11.5 *msec* passed since start.

Drift is clearly seen here. So the temperature at point ***i*** is the lowest one and drops its temperature fasted, than any other one. We would like to remind, that time between beam trains in ILC is ~200 ms for 5 *Hz* operation.

We recommend arranging this side towards the target, so the heating condition will be relaxed substantially. Further time development up to 80 *ms* is shown in Fig.48 below

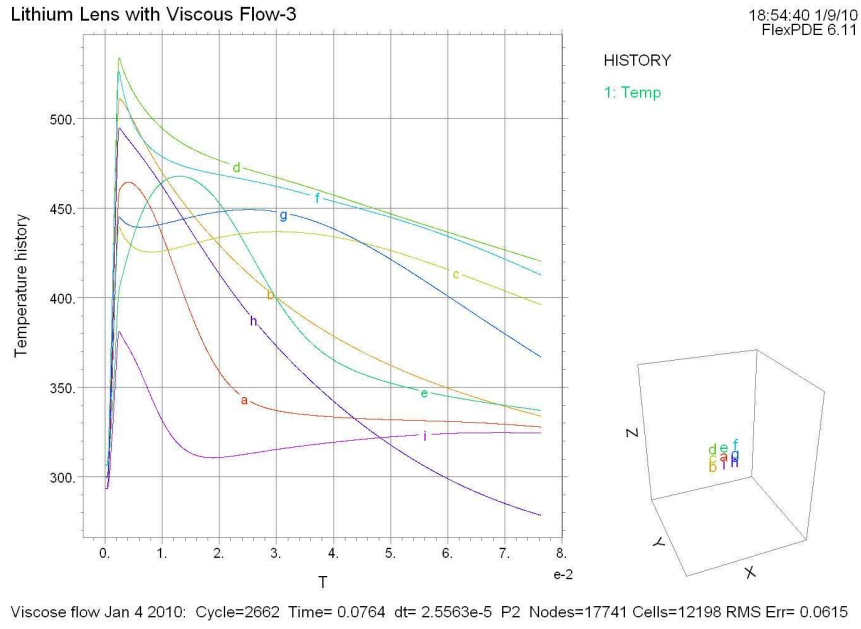

Figure 48: Temperature in Celsius in this plot. 76.4 *msec* passed.

One can see that temperature in point ***h*** is relaxing to the inlet temperature (250 Deg) in quickest manner. This is due to the liquid flow. Appropriate temperature profile in all cross section is shown in Fig below. A "tongue" with lowest temperature can be explained by flow from inlet tube, which located close to this side.

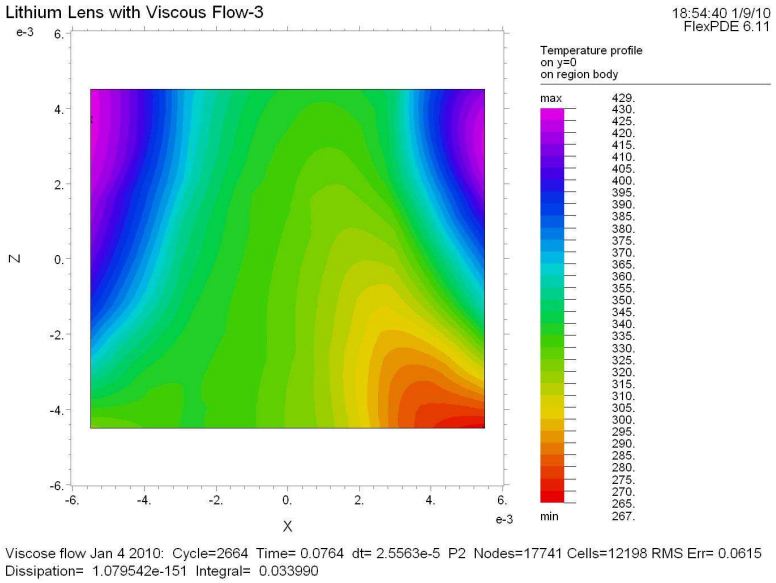

Figure 49: Temperature is given in Celsius; temperature kept fixed at the entrance and exit only. 76.4 *msec* passed.

In other scenario the temperature of all walls kept fixed at 480 ^{o}K. As the speed of liquid reaches 100 m/s by magneto effect, that means that the distance between the wall and center of lens, ~0.5 cm liquid passes in $\tau \cong 5 \cdot 10^{-3} / 100 = 0.05 ms \equiv 50 \mu s$. As the pulse duty is 2.3 *ms*, this effect should be significant. Result is shown in Figure below.

One can see that high temperature liquid moved to the central region. Temperature rise is substantially lower, than in first case and cooling is going much more effectively.

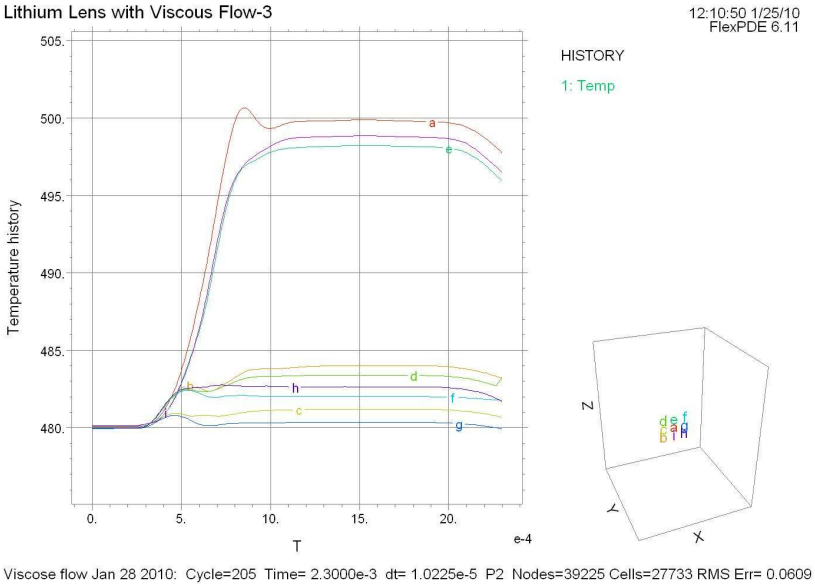

Figure 50: Temperature history at the same points, when the walls temperature kept constant at 480^{o}K.

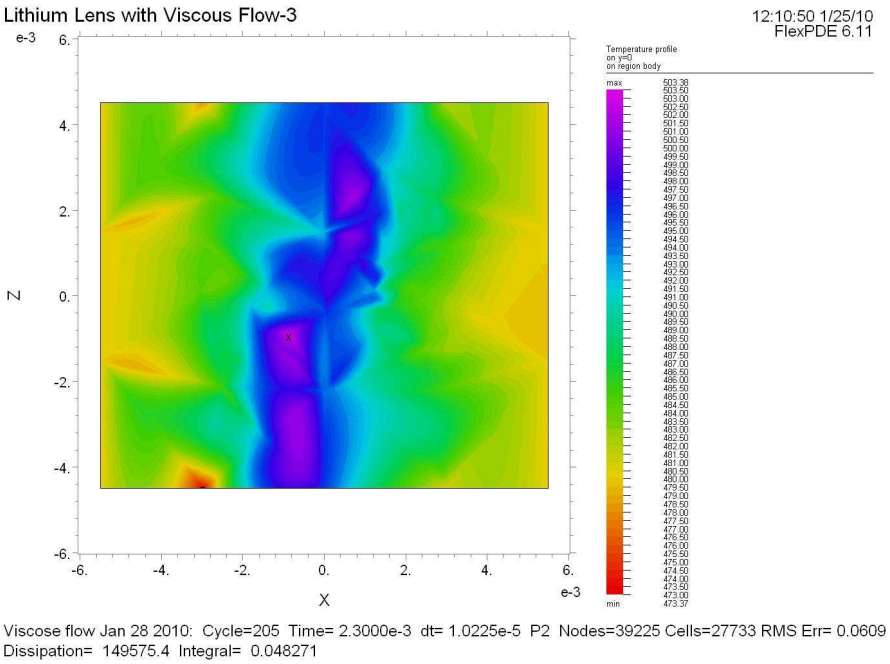

Figure 51: Temperature profile for the temperature kept 480 ^{o}K at the walls

DISCUSSION

The magneto-hydrodynamic problem of Lithium flow is extremely complicated for numeric modeling due to nonlinear nature of equations involved. Low viscosity of liquid Lithium (as it is about the same as it is for hot water) magnifies difficulties of problem modeling. Lithium flow in the volume is pretty turbulent for pressure drop in the model within fraction of atmosphere. So some stabilizing mechanisms typical for numeric modeling should be used here. Reduction of pressure drop (inlet/outlet) to 0.01 atm allows steady laminar flow.

Meanwhile in the big picture, the following was identified during modeling: when the current starts running through Lithium, it generates a substantial pressure difference *across* the flow which reaches few tens of atmospheres. This pressure rise is defined by velocity-dependent part as

$$\sim (\vec{j}\times\vec{B}) \cong \sigma\cdot(\vec{v}\times\vec{B})\times\vec{B}\,.$$

Sequentially, the velocity of liquid reaches tens of meters per second (~100 *m/sec* max) inside small volume of lens. This rapid vortex motion raises dynamic pressure a few times compared to initial one, but liquid is rapidly mixing, caring cold fractions, which were in contact with walls, to the central region. We can treat this process as forced convectional cooling. Here is the key difference between solid and liquid Lithium: in case of solid, compression of Lithium rod in radial direction transferred to longitudinal direction (towards windows) according to atomic forces according to Poisson ratio. Tendency of radial divergence of material is suppressed by atomic forces inside solid, so we expect that in case of liquid the hit of window is smaller. In any case the pressure at the surface of the window is ~ 3 times lower, than the one in central region.

One can estimate, that velocity ~100 *m/s* will mix the Lithium volume within time frame $\sim r/v \approx 5\cdot 10^{-3}[m]/100[m/s] = 0.05ms \equiv 50\mu s$, which is forty times less than the feeding electric pulse duration. So roughly, the temperature gain after passage of single 1*ms*-long train could be considered as the one distributed over the whole Lithium volume. As the one is ~6 cubic

centimeters, and the total energy deposited in a volume by Ohmic losses calculated to be ~682 *Joules*, the temperature gain could be majoretted as

$$\Delta T \cong \frac{Q}{\rho \cdot V \cdot c_V} \cong \frac{682}{0.5 \cdot 10^3 \cdot 6 \cdot 10^{-6} \cdot 4.4 \cdot 10^3} \cong 50°K\,.$$

Direct calculations show, that maximal temperature rise is somewhere around 20^oK in scenario when the walls are kept at a fixed temperature.

So the effect of *magneto* in liquid Lithium helps in cooling the volume. By keeping the temperature of the walls just above the melting point, situation with cooling could be relaxed further.

One can consider even more radical scenario, when the Lithium is melted by the electric pulse itself, while between pulses it remains in dual hard and liquid phase.

SUMMARY

Lithium lens consideration, which includes magneto-hydrodynamics in absence of beam, indicates interesting phenomena in liquid Lithium lens while magnetic pressure is acting to the flow. In particular, we discovered vortex circulation of liquid Lithium due to magnetic force. This effect of *magneto* helps in drastic reduction of temperature in central region of windows, thanks to forced mixing. Presence of buffer toroid-like volumes is desirable for this process.

Motion of Lithium in system is deeply turbulent, which makes modeling extremely difficult, with some stabilizing mechanisms and tuning model, the solution could be found even for Re~5000.

Calculated pressure and temperature profiles and some optimization confirm that parameters of lens are technically reasonable. Generally, the temperature rise is below 50 ^{o}C coming to a total of ~100 ^{o}C with beam as the beam duty of train is ~1 msec –is less than the time when feeding current applied (and when effective convectional mixing mechanism is in action) .

We recommend increase of length of space occupied by Lithium (in direction along the beam pass) to ~1 *cm* (from~0.6cm in [1]). This brings reduction of current to ~70 kA.

We also slightly modified the configuration of junction between Lithium cylindrical container and the buffer toroid-like volume. This improved linearity of integrated field as function of transverse coordinate.

In following publications we will represent the beam action to the processes; all computer code preparations are done for this. Saying ahead, the beam-train deposited rise of temperature stays below 100 degrees in mostly critical locations (entrance window). Very short beam pulse introduces new phenomena in the process, however.

Numerical code developed allows further investigation of Lithium lens dynamics and easy modification of geometry. Mostly time was spent developing proper boundary conditions.

Stress-strain in windows, Shock waves and Cavitations introduced by the beam will be described in separate publication. Saying ahead we express assurance that there are no apparent limitations for usage of lens with liquid Lithium for positron production busyness.

Usage of FlexPDE computer code looks more or less adequate here as there are no visible nuances; although at some stage the usage of more advanced codes (such as ANSYS) may be necessary. Best test for liquid Lithium lens remains the full fabrication of lens with power supply and a live test.

Work supported by DOE grant DE-AC02-98CH10886

REFERENCES

[1] A.Mikhailichenko, "*Lithium Lens* (I)", CBN 09-4, Aug 2009, 17pp., available at http://www.lepp.cornell.edu/public/CBN/2009/CBN09-4/CBN%2009-04.pdf

[2] A.Mikhailichenko, "*Lithium Lens for Positrons and Antiprotons in Comparison*", CBN 09-8. http://www.lepp.cornell.edu/public/CBN/2009/CBN09-8/CBN%2009-08.pdf

[3] L.D.Landau, E.M.Lifshits, "*Hydrodynamics (Fluid Mechanics)*", (Course of Theoretical Physics, VI), Oxford: Pergamon Press, (1982)

[4] L.D.Landau, E.M.Lifshits, "*Electrodynamics of Continuous Media*", (Course of Theoretical Physics, VIII), Oxford: Pergamon Press, 1960.

[5] W.F.Hughes, J.A.Brighton, "*Fluid Dynamics*", Schaum's outline series, ISBN 0-07-0311117-X.

[6] R.W.Ohe (Ed..) Handbook of THERMODYNAMICS AND Transport Properties of Alkali Metals" Intern. Union of Pure and Applied Chemistry Chemical Data Series No.30. Oxford: Blackwell Scientific Publ.

[7] Y.Ito et al., International Journal of Thermophysics, Vol 10, No1, 1989.

[8] PDE Solutions, FlexPDE,